Estimating volumes of supraglacial lakes on the AIS

MSc Thesis Geosciences and Remote Sensing

Comparing satellite-based and model-based techniques for estimating water volume of supraglacial lakes on the Antarctic ice sheet

Wytse Petrie 4394704

Thesis committee:

Dr. Stef Lhermitte	**TU Delft, chair**
Dr. ir. Bert Wouters	**TU Delft**
Ir. Sophie de Roda Husman	**TU Delft**

19 September 2022
Delft University of Technology, Faculty of Civil Engineering and Geosciences
Stevinweg 1, 2628 CN Delft, The Netherlands

Abstract

Disintegration of Antarctic ice shelves can induce devastated consequences for the environment and human infrastructure in the form of an increase of the global mean sea level. One of the causes of an ice shelf break down is hydrofracturing due to the mass load of supraglacial lakes. The top of the snowpack melts and the meltwater flows to a local depression where it accumulates and forms melting ponds. Detecting and quantifying the depth of these supraglacial lakes will increase the knowledge on the evolution of supraglacial lakes. Satellite remote sensing techniques are able to determine the volume of individual ponds. However, these methods have their limitations in calculating the depth and area per lake. Regional climate models are capable of estimating the total volume of meltwater within a certain area of interest, but have until now not been able to measure the depth and area of separate supraglacial lakes with certainty. This research study focused on highlighting the limitations of and developing possible improvements for three climate-based and satellite-based methods for comparing them to one another. The first method made use of Sentinel-2 scenes and a threshold-based classification to calculate the water extent and the water depth was calculated by use of band values and by knowing both the volume can be estimated. The second method made use of Sentinel-1 and Sentinel-2 images to classify areas containing water over a biweekly interval. A new method, denoted as the kernel method, was developed for measuring the depth of each detected lake with a lake mask and a digital elevation model. The volume is subsequently derived from the water extent and depth. Snowmelt, refreezing, precipitation and snowfall from a regional climate model, RACMO, was applied to estimate the total volume of meltwater within a catchment. With a digital elevation model a routing is determined to visualize where the calculated meltwater accumulates and subsequently the depth and area were computed. Based on comparing the water extents over the period of 2016-2021 on the Nivlisen Ice Shelf the following can be concluded: the climate model-based method cannot produce realistic water extents (the results were ten times larger than the satellite-based methods); the different classification methods have similar outcomes, the thresholds of the method using solely Sentinel-2 are preferred; The satellite methods are limited by clouds and frozen ice lids. The results of the water extents indicated unnatural large depths (average $+30\ m$) and that the satellite remote sensing methods produce water extent in the same order of magnitude. In addition, the kernel method showed potential, since it can be executed without non-optical satellite data. However, in order for it to improve, the size of the kernel needs to be optimised. The total volumes are in the same magnitude range, but the climate data method overestimates (getal) due to the fact that the maximum value is chosen within the biweeks. In addition, this study's resulting volumes are close to the values computed by Van der Zalm (2020) and Dell et al (2020), which increases the confidence in the results. However, a problem that arose is the absence of a ground truth to accurately compare the results with and therefore it is recommended to possibly compare the data to that of an altimeter. Additional improvements can be made in kernel size optimization based on the middle line of the lakes and developing a method to correctly locate and calculate the depth of water using a total runoff and a digital elevation model.

List of Figures

List of Tables

Contents

1 Introduction

Global climate change is accelerating and the temperatures are arising around the Antarctic Ice Sheet [Meredith and King, 2005]. Several studies indicated ice shelf disintegration due to hydrofracturing resulted from melting ponds [Banwell et al., 2013], [Bell, 2018], [Cook and Vaughan, 2010], [Rignot et al., 2004], [Scambos et al., 2004]. The ice shelves buttresses the ice flow into the ocean, a collapse will accelerates this flow and causes an increase of ice mass loss. The ice flowing into the ocean will lead to an in increase of global mean sea level. Recent years there has been development in estimating the location and volumes of the supraglacial lakes using satellite remote sensing techniques [Moussavi et al., 2020], [Dirscherl et al., 2021b]. In addition, research is done in calculating meltwater based on regional climate models [Hu et al., 2021], [van Wessem et al., 2018]. Better understanding and improving existing methods and developing new techniques for estimating volume and position of these supraglacial lakes increase insights on the vulnerability of ice shelves and the AIS and hence on the global mean sea level. By comparing these with each other, this becomes more visible and improvements can be made. In addition, new techniques are developed and applied to make the estimates more accurate. This will lead to a better understanding of the stability of the ice shelf. Getting a sharper handle on the influence of meltwater lakes on the instability of Antarctic ice shelves depends on accurately mapping presence and volume of meltwater. Increasing the predictibility of the water quantity and location reduces the uncertainty in the vulnerability of the ice shelf and also the change in global sea level, which helps in making more accurate sea-level projections.

1.1 Antarctic Ice Sheet

The Antarctic Ice Sheet is the biggest of the two polar ice caps on Earth. The ice sheet contains around 98 percent of the total continent. The ice sheet has an average thickness of approximately 2 km and covers an area of almost 14 million kilometers. The 26.5 km^2 of ice are able to rise the sea level 58 m [Fretwell et al., 2013].

Studying the behavior of Antarctica is very interesting in connection with its influence on sea level and the warming climate. In addition, this becomes more urgent when considering the topography of Antarctica (figure 2.1.4). From this image it can be obtained that a relatively large part behind the boundary with the sea is below sea level. In the event that the boundary disappears, a large part of Antarctica will become submerged, resulting in an acceleration of the ice volume.

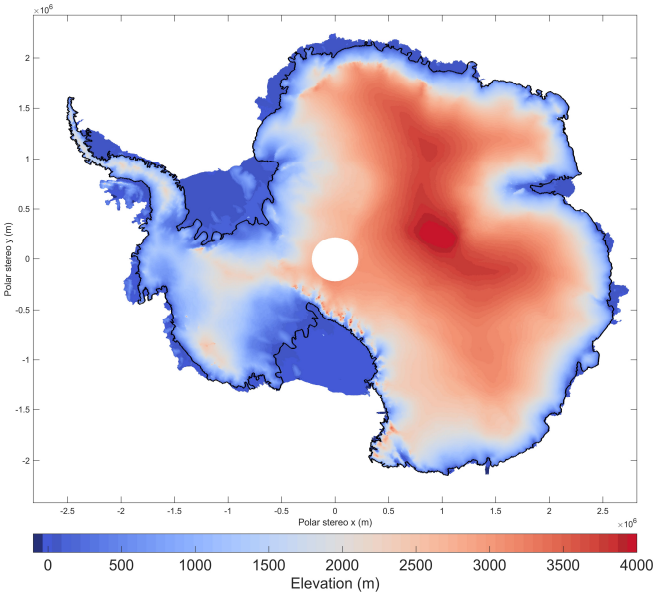

The e

Figure 1.1.1: Elevation of Antarctica, given in meters.

Due to the fact that the climate is changing, the global mean temperature and the global mean sea surface temperature are increasing. The global rise in temperature is causing growth in surface melt and basal melt. Therefore, the behavior of the Antarctic Ice Sheet (AIS) is a crucial measure of climate change. The AIS is containing a volume of ice large enough to raise the global sea level by approximately 58 meters [Fretwell et al., 2013]. During the period between 2006 and 2015, the AIS mass loss has caused a sea level rise of $0.43 \pm 0.05\ mm\ yr^{-1}$ and is currently increasing [Church et al., 2013]. The global mean sea level rise is quantified in the latest report of the Intergovernal Panel on Climate Change (IPCC) using multiple Shared Socioeconomic Pathway (SSP) scenarios and the influence of mass loss of the AIS. The impact on the mean global sea level of the AIS for the different scenarios is estimated at 0.03–0.27 m (SSP1–2.6), 0.03–0.29 m (SSP2–4.5), and 0.03–0.34 m (SSP5–8.5) [Church et al., 2013]. According to the IPCC, there is large uncertainty in the amount sea level rise, the greatest influence on which is the contribution of the ice shelves on Antarctica.

1.1.1 Ice shelves

Ice shelves are floating ice formations that are permanently attached to a landmass. The location where the ice sheet and the ice shelf are connected is called the grounding line (figure 2.1.6). Most of the ice shelves on Antarctica are located around the Antarctic Ice Sheet. The ice flows from the glaciers towards the sea. If the ocean water is cold enough the ice will not melt immediately and will float up on it. Over time more ice will flow toward the sea and the floating ice mass will expand. The ice shelves are gaining weight due to these ice flows and lose mass by the calving of the ends of the floating ice, dynamic stability is derived. The volume of ice shelves and the sea level are inversely proportional to each other, however, this relation is not direct. Since the shelves are already floating on top of the ocean, the disintegration of the shelves will not cause a rise or drop in the water level (Archimedes). These ice shelves have a so-called buttressing effect, which regulates the ice flow discharge into the ocean [Fürst et al., 2016]. The ice shelf buttresses the ice flow from the glacier into the water and slows down the ice discharge. The ice shelf exerts a back pressure on the land ice. The velocity of the ice will increase as a consequence of shrinking ice shelves with an increase in seawater level as result. The faster ice flow will induce this process and so on.

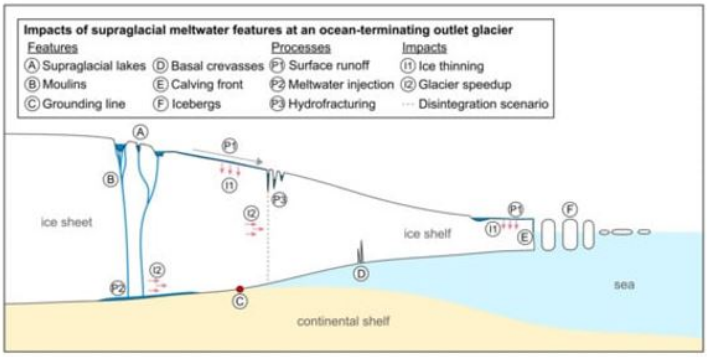

Figure 1.1.2: Schematic of different processes around the ice shelf and ice sheet [**?**]

In recent decades, several major disintegrations of ice shelves have been observed, which have multiple natural causes. First, the ice shelves become unstable, after which they can be disintegrated, which is a process that can take place over years to decades. The instability of an ice shelf is driven by thinning as a consequence of different natural processes. The ice shelf melts at the bottom because the temperature of the water is above the melting point, which is called basal melt [the IMBIE team, 2018]. Ice dynamics can cause cracks or fractures in the ice shelf [Lhermitte et al., 2020]. Warm air can melt the snow on top that results in accumulation of water into pre-existing crevasses, cracks, rifts, or depressions and form supraglacial lakes which causes hydrofracturing [Munneke et al., 2014]. These mechanisms are natural, but due to the warming of the Earth and climate changes these processes are accelerated [Rignot et al., 2019]. A warmer climate produces warmer water, higher ice velocities, and warmer air, which in turn increases basal melt, size of cracks, and surface melt. These processes result in a thinner ice shelf, which in turn causes more instability.

The formation and impact of supraglacial lakes are currently not completely understood, but are crucial for understanding the Antarctic Ice Sheet.

1.1.2 Supraglacial Lakes

Supraglacial lakes, as the name already implies (supra means on top), are water bodies on top of a glacier. During the summer months, snow melts and accumulates into pre-existing crevasses, cracks, rifts, or depressions, which cause the formation of so-called supraglacial lakes. The ice pack is divided into three stages: surface snow, firn, and ice indicated in figure 2.1.7. Firn is the intermediate stage between fresh snow and glacial ice. The firn layer increases in density with depth due to the compaction of the snow/ice. In the snow and upper firn layer, there are porous holes filled with air, these spaces can act as a buffer. During the summer, when the temperature exceeds the melting temperature, snow melts and can flow into these spaces and refreezes. As long as the volume of the pore space is bigger or equal than the refreezing meltwater, the firn layer's buffer is capable of storing all the water. The pore space is dependent on the snowfall rate: the more fresh snow, the more pores. However, if the layer is saturated and the meltwater has no other place to go, the meltwater flows into existing crevasses, rifts, or cracks. If there are no existing fractures, the firn layer will be flooded, where the drainage is insufficient and thus meltwater lakes can form in places where the surface is lower, which is called a depression. Based on recent studies the mean water depth of supraglacial lakes on Antarctica does not exceed 6 m [Pope et al., 2016], [Fricker et al., 2021], [Arthur et al., 2020].

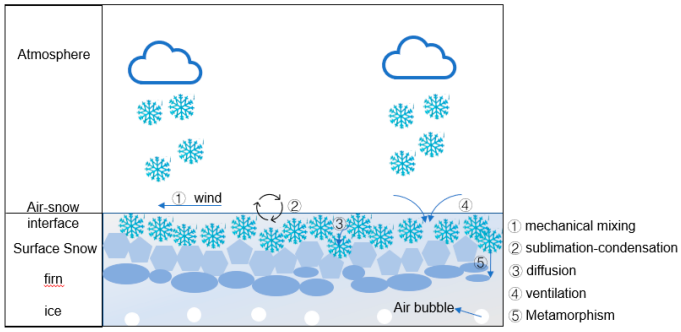

Figure 1.1.3: Schematic representation of the firn layer

Then it can force crevasses through tensile stresses. When the meltwater exceeds a 90% of the volume of the crack, it will become too heavy and exerts too much stress on the fracture and it will become wider and deeper [Lai, 2020]. This can lead to drainage and create flexure stresses on ice shelves. These flexible tensile stresses can be significantly large and induce neighboring lakes to drain as well through a chain reaction process, depending on the distribution and the depths of these lakes [Banwell et al., 2013]. The chain reaction of supraglacial lakes can cause a rapid disintegration of an ice shelf, which has for instance happened to the Larsen B ice shelf [Scambos et al., 2004]. Better understanding and improving the estimation of the volume and the locations of these supraglacial lakes could increase insights on the vulnerability of ice shelves and the AIS and hence on the global mean sea level.

1.2 Estimating volume of supraglacial lakes

There are three well-known methods to estimate the extent and volume of meltwater lakes over the Antarctic ice shelves: automatic weather stations, regional climate models, and satellite observations. The methods use different techniques for computing the area, the depth and the volume of those ponds. The methods are based on in-situ, climate and satellite data and during last years there a lot of developments have been made in this particular field of interest.

The Automatic weather stations measure different quantities , including surface melt, constantly at the location of the station [Jonsell et al., 2011]. These observations can be seen as true, since they are directly measured. It is not feasible to create a network of AWS that is able to monitor all the meltwater on

the Antarctic Ice Shelves. There are currently 57 AWS on Antarctica, which all provide meltwater point-measurements.

Recent advances have been made in estimating the surface melt using a climate model using the regional atmospheric climate model (e.q. Modèle Atmosphérique Régionale (MAR) and Regional Atmospheric Climate Model (RACMO)). The forcing is used to determine snowmelt, refreezing, temperature, and incoming shortwave radiation [van Wessem et al., 2018]. According to studies, it is shown that RACMO data can under-estimate surface melt by 30 to 50 %, and the biggest difference is near the grounding line [Lenaerts et al., 2017], [Lenaerts et al., 2018]. A reason for this phenomenon is that the resolution of the RACMO is too coarse to estimate the föhn effect of the adiabatic winds sufficient enough [Trusel et al., 2011]. Over the last years, modeling the flow of meltwater and therefore determining the location of accumulation have improved. Scientists modeled the formation of supraglacial lakes based on a mathematical model, which includes 3D processes such as water routing and channel erosion [Buzzard et al., 2018] and [Buzzard and Robel, 2020].

Different is processing satellite imagery to analyze present meltwater networks, as done by [Dell et al., 2020]. This work is further expanded by including topographical information on the ice shelf and by comparing the results to a regional climate model [Geerten, 2020].

Determining the area and depth of the lakes using satellite data has improved over the last few years using classification methods. The melting ponds are often classified from data of Sentinel-2 and Landsat 8 based on reflectance properties [Stokes et al., 2019], [Moussavi et al., 2020]. In order to improve the results Sentinel-2 data is trained using a digital elevation model (DEM) [Dirscherl et al., 2020]. For determining the depths Sentinel-2 and Landsat 8 can be used as well [Moussavi et al., 2020]. Another way to define the depth is by utilizing the topography to calculate the mean depth [Howat et al., 2019] and to determine the depth via ICESat-2 data [Fair et al., 2020]. One advantage to using optical data is that it is easy to validate whether the water is properly classified. A disadvantage is its sensitivity to clouds, as there are many clouds present around the ice shelves on the AIS.

Recent studies (e.g. GILBERT AND KITTEL 2021, [Trusel et al., 2011], DECONTO AND POLLARD 2016) showed that ice shelf instability can lead to a significant inscrease in the contribution of the AIS to sea level rise. This involved examining how to determine surface meltwater as accurately as possible based on climate models. In addition, consideration has been given to how meltwater will flow across the surface and accumulate into a lake. Various ways of using satellite observations to allocate the lakes and determine their volume have also been devised. The main focus has been on detecting water and there is more room for improvement in terms of estimating the water depths and so the volumes. Ultimately, the volumes of supraglacial lakes are essential to the vulnerability of an ice shelf. The three above-mentioned methods of estimation volumes have each their downsides, advantages and problems. By comparing these with each other, this becomes more visible and improvements can be made. In addition, new techniques are developed and applied to make the estimates more accurate. This will lead to a better understanding of the behavior of the ice shelf. Getting a sharper handle on the influence of melt lakes on the instability of Antarctic ice shelves depends on accurately mapping presence and volume of meltwater. Reducing the uncertainty about the water quantity reduces the uncertainty in the behavior of the ice shelf and also of the sea level. Comparing different methods gives a better understanding of this end, which helps in making more accurate sea-level projections.

1.3 Research question

The object of this research is to improve satellite-based methods and a model-based method determining the extent and volume of supraglacial lakes on Antarctica. This is done by comparing the area, depth and volume of the melting ponds calculated using three methods. Due to the comparison a better understanding of the limitations of the methods is profound and possible solutions can be applied. A more accurate mapping and estimation of the volume of supraglacial lakes increases the insight in the stability and possible vulnerability of the ice shelf. The objective of this research will be reached by answering the following research question:

What are the possibilities and limitations of estimating the water volume of supraglacial lakes on Antarctic Ice Shelves using satellite-based and model-based techniques?

To solve this research question, three sub-questions are presented that need to be answered in order to answer the main question.

i. What are the spatiotemperal patterns in detecting lake presence between the different satellite methods

ii. How can meltwater volumes be derived using non-optical satellite data?

iii. What are the possibilities of determining the volume of individual water bodies using a Regional climate Model

2 Background

2.1 Antarctica Ice Sheet

The Antarctic ice sheet is the biggest of the two polar ice caps on Earth. The ice sheet contains Around 98 percent of the total continent. The ice sheet has an average thickness of approximately 2 kilometers and covers an area of almost 14 million kilometers. The 26.5 cubic kilometers of ice are able to rise the sea level 58 meters [Fretwell et al., 2013].

Studying the behavior of Antarctica is very interesting in connection with its influence on sea level and the warming climate. In addition, this becomes more urgent when considering the topography of Antarctica (figure 2.1.4). From this image it can be obtained that a relatively large part behind the boundary with the sea is below sea level. In the event that the boundary disappears, a large part of Antarctica will become submerged, resulting in an acceleration of the ice volume.

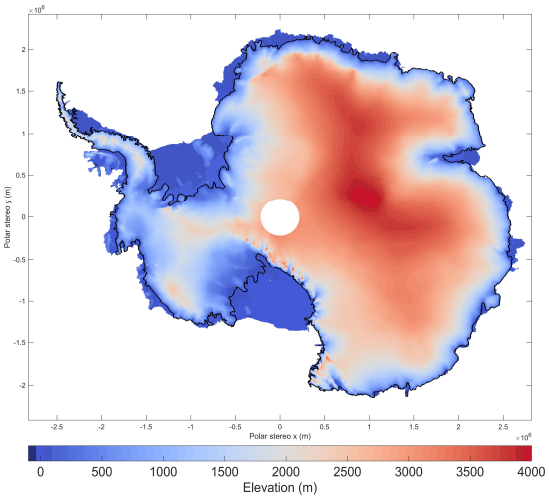

The e

Figure 2.1.4: Elevation of Antarctica, given in meters.

One way to monitor the change in the amount of ice is to compute the Surface Mass Balance (SMB). It is the difference between what increases the volume of ice, precipitation, and what decreases, Sublimation and Runoff (equation 3).

$$SMB = Precipitation - Sublimation - Runoff \tag{1}$$
$$= (Snowfall + Rainfall) - Sublimation - (Melt + Rainfall - Refreezing) \tag{2}$$
$$= Snowfall - Melt - Sublimation + Refreezing \tag{3}$$

If the value of SMB is larger than zero, it means that there is more surface mass added to the system than it is lost, this is called the accumulation zone. The area with a negative SMB is called the ablation zone. The mass change of the ice sheet is calculated by subtracting the ice discharge (D), caused by iceberg calving and marine melt, from the SMB (equation 4).

$$Mass\ change = SMB - D \tag{4}$$

A Negative mass change means a decrease in ice mass since the discharge is greater than the SMB. In the last several years the mass of the Antarctic Ice Sheet has changed dramatically. According to the results of NASA's twin NASA/German Aerospace Center's twin Gravity Recovery and Climate Experiment (GRACE) satellites, the AIS loses 125 gigatons of ice per year over the period 2002 to 2016, see figure 2.1.5. This mass flux causes a global sea level rise of 0.35 millimeters per year [Tapley et al., 2019]. From the image, it can be obtained that in the West the mass change is strongly negative, while in the other parts the change is slightly positive or negative. The colored gray parts are ice shelves and GRACE did not measure those.

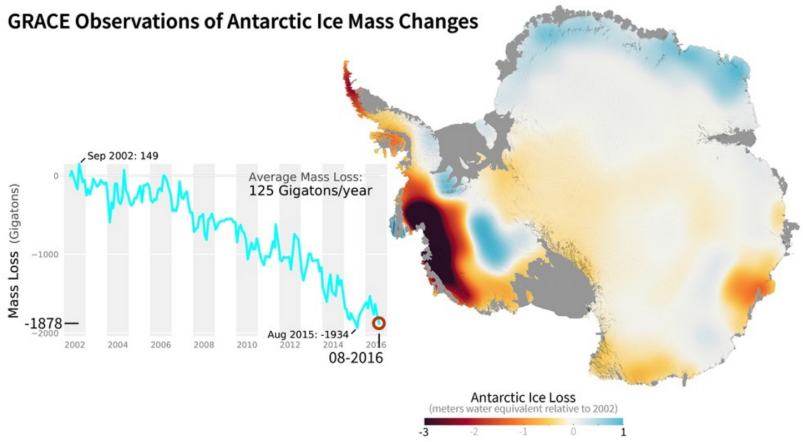

Figure 2.1.5: Antarctic Ice Mass changes according to GRACE observations from 2002 to 2016 with spatial variability

2.1.1 Ice Shelves

Ice shelves are ice sheets connected to a landmass, floating on the sea. The location where the ice sheet and the ice shelf are connected is called the grounding line. Most of the ice shelves are located around the ice masses of Antarctica (figure 2.1.6. The ice flows from the glaciers towards the sea. If the ocean water is cold enough the ice will not melt immediately and will float up on it. Over time more ice will flow toward the sea and the floating ice mass will expand. The ice shelves are gaining weight due to these ice flows and lose mass by the calving of the ends of the floating ice, dynamic stability is derived. As already mentioned the decrease of ice shelves have a positive impact on the sea level, however, this relation is not direct. Since the shelves are already floating on top of the ocean, the disintegration of the shelves will not cause a rise or drop in the water level (Archimedes). The ice shelf buttresses the ice flow from the glacier into the water, because of this the stream will be less fast. The ice shelf exerts a back pressure on the land ice. The velocity of the ice will increase as a consequence of shrinking ice shelves with an increase in seawater level as result. The faster ice flow will induce this process and so on.

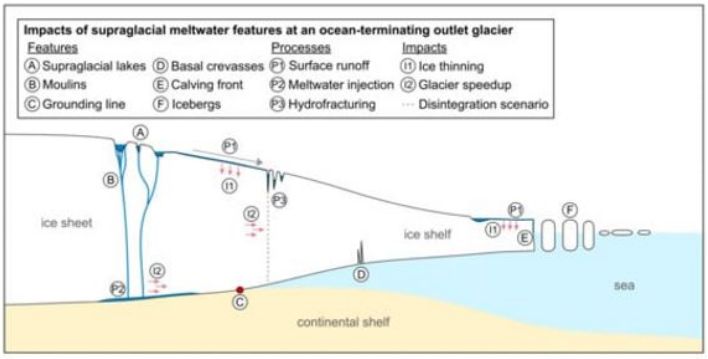

Figure 2.1.6: Schematic of different processes around the ice shelf and ice sheet, [Dirscherl et al., 2021b]

In recent decades, several major disintegrations of ice shelves have been observed, which have several causes. First, the ice shelves become unstable, after which they can be disintegrated, this process can take place over years to decades. The driver of this instability is global warming and climate change [Rignot et al., 2019]. The ice shelf melts at the bottom because the temperature of the water is above the melting point [the IMBIE team, 2018]. In addition, ice dynamics can cause cracks in the ice [Lhermitte et al., 2020] and warm

air can melt the top of the ice shelf [Munneke et al., 2014]. A warmer climate produces warmer water, higher ice velocities, and warmer air, which in turn increases basal melt, size of cracks, and surface melt. These processes result in a thinner ice shelf, which in turn causes more instability. During this research, we will be focusing in particular on the formation of supraglacial lakes. When the top of the snow layer melts, the meltwater accumulates in depressions or cracks, and in this way a lake can be formed. The lake exerts pressure on the surface ensures the ice shelf to be potentially unstable [Urruty et al., 2022].

2.1.2 Supraglacial lakes

Supraglacial lakes, as the name already implies (supra means on top), are water bodies on top of a glacier. The water comes from snow surface melt. The ice pack is divided into three stages, surface snow, firn, and ice indicated in figure 2.1.7. Firn is the intermediate stage between fresh snow and glacial ice. The firn layer increases in density with depth due to the compaction of the snow/ice. In the snow and upper firn layer, there are porous holes filled with air, these spaces can act as a buffer [Munneke et al., 2014]. During the summer, when the temperature exceeds the melting temperature, snow melts and can flow into these spaces and refreezes. As long as the volume of the pore space is bigger or equal then the refreezing meltwater, the firn layer's buffer is enough. The pore space is dependent on the snowfall rate, the more fresh snow the more pores [Lai, 2020]. However, if the layer is saturated and the meltwater has no other place to go, the meltwater flows into existing crevasses, rifts, or cracks. If no existing fractures, the firn layer will be flooded, where the drainage is not enough, and thus meltwater lakes can form in places where the surface is lower (depression). Then it can force crevasses through tensile stresses [Munneke et al., 2014]. When the meltwater exceeds a

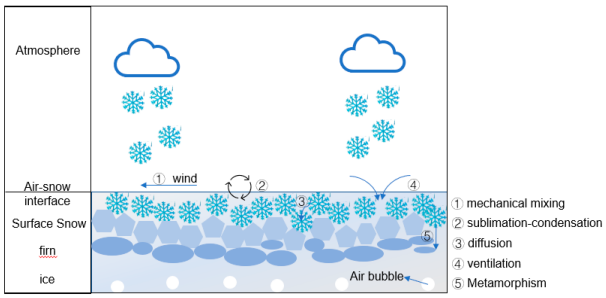

Figure 2.1.7: Schematic representation of the firn layer, [Munneke et al., 2014]

certain amount (90% of the volume of the crack), it will become too heavy and exerts too much stress on the fracture and it will become wider and deeper, see figure 2.1.8. If this happens enough and the cracks are being filled, these cracks can grow to the bottom of the ice shelf and cause collapse (Lai).

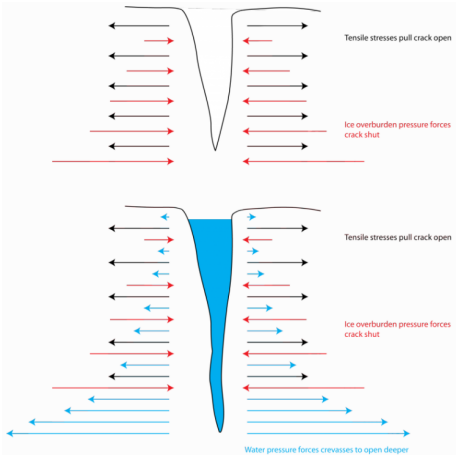

Figure 2.1.8: Representation of the cracks being filled with water and grow

2.2 Satellite Remote Sensing

Remote sensing is the process of detecting and monitoring the physical characteristics of an area by measuring its reflected and emitted radiation at a distance. Sensors collect remotely sensed images, which help researchers "sense" things about the Earth. In the case of satellite remote sensing, the object that measures is a satellite. There are mainly two different types: Passive remote sensing and Active remote sensing, see figure 2.2.9. Passive sensors use radiation emitted or reflected by the object or the surrounding areas, in most cases this is the reflected sunlight. Active sensors emit energy by themselves and detect and record the reflected or backscattered energy.

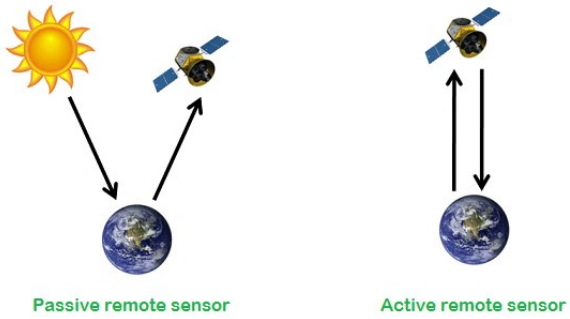

Figure 2.2.9: Schematic image of passive and active remote sensing

The energy produced by the source is called electromagnetic energy, which is produced by the vibration of charged particles and travels in the form of waves through the atmosphere and the vacuum of space. For every object with a temperature of more than 0 Kelvin is able to radiate energy and thus electromagnetic waves.

The amount of energy that an electromagnetic wave contains depends on the wavelength. The entire range of wavelengths is known as the electromagnetic spectrum, see figure 2.2.10.

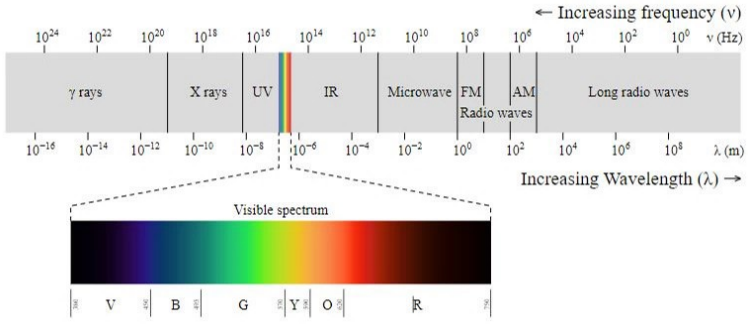

Figure 2.2.10: Electromagnetic spectrum with associated frequencies and wavelengths

The result of an satellite image is grid composed of pixels. A grid can be seen as collection of tiles, named grid points, in longitude and latitude direction. Each grid point represents a certain value or multiple values and has a certain area. Together the grid forms a raster layer. The size of each pixel is called the spatial resolution and determines the smallest particle that can be measured. The temporal resolution defines the rate of observing the same area. There is a trade-off between spatial and temporal resolution, since a higher

spatial resolution leads to a smaller field of view, which results in a lower temporal resolution. Spectral resolution signifies the sampling rate and wavelength in which the sensor collects the information about the scene [Kotawadekar, 2021]. Every satellite has it's own characteristics about these types of resolutions. Two types of satellite are Synthetic Aperture Radar (SAR) and Multi-spectral. Radar remote sensing operates in microwave part of the spectrum, which is between wavelengths of 1cm and 1 meter. The multispectral satellite uses, as the name suggests, multiple portions of the spectrum.

3 Study area and data

In this chapter, we zoom in on the ice shelf of interest (Nivlisen) and its surroundings. In addition, an overview of the types of data used in this study is provided.

3.1 Nivlisen Ice Shelf

The study area of interest for this research is the Nivilisen Ice Shelf. The ponds on the Nivlisen ice shelf were researched from the period 2016-2021. Water volume estimations of these lakes have been done in prior research for this particular area (BRONNEN). The ice shelf is located in the Dronning Maude Land in the north of Antarctica. Nivlisen has an area of around 7300 km^2 which stretches from the west to the east and from the north to the south over approximately 80 and 130 kilometers, respectively [Horwath et al., 2006]. The ice shelf is caught between the Southern Ocean in the north and high steep mountains in the west [Howat et al., 2019]. The Vigridsen (west) and Lazerivsen (east) are separated from Nivlisen by to two ice-rises, Djupranen and Leningradkollen [Lindbäck et al., 2019], as indicated in figure 3.1.11.

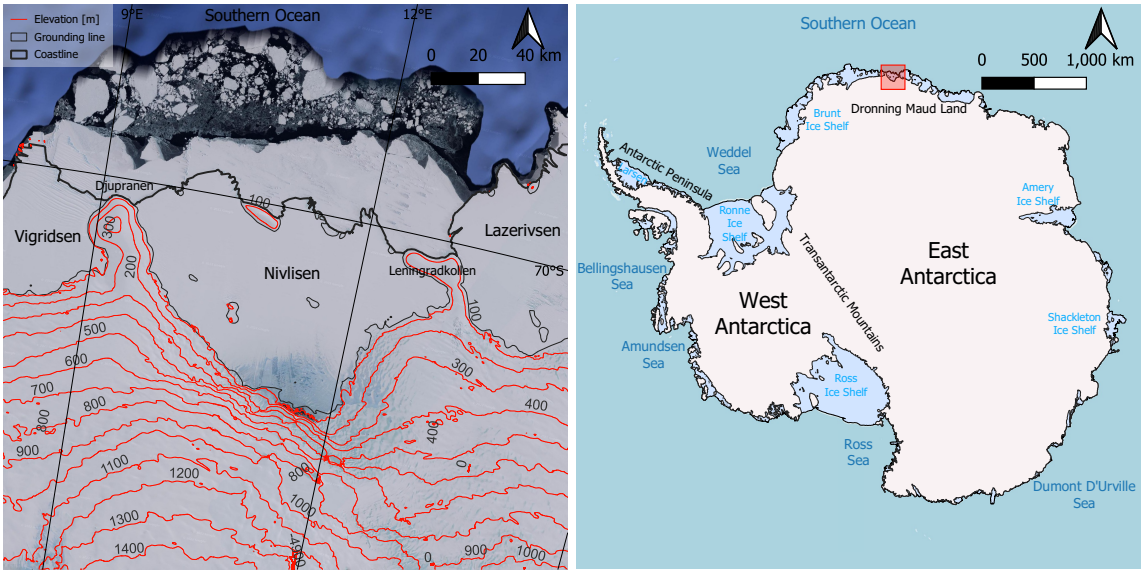

(a) (b)

Figure 3.1.11: Study area of Nivlisen (a), indicated are the adjecent ice shelfs, ice rises and elevation contour lines. Location of Nivlisen on Antarctica (b) in the red box.

The ice flow velocity is around 80 meters per year, averaged over the whole shelf [Rignot et al., 2011]. The global sea level will be potentially elevated by 8 cm if Nivlisen would be disintegrated. The ice shelf contains a drainage basin of 27,000 square kilometers [Rignot et al., 2019]. Climate and Surface Mass Balance (SMB) gradients are strongly fluctuating due to the elevated topography of the ice rises [Lenaerts et al., 2014]. According to Rignot et al. (2013), using satellite information, the estimated SMB was 1.8±0.3 Gt yr^1 averaged over the period 1979–2010. The grounding line flux was 3.9±0.8 $Gt\ yr^1$ and the calving flux was 1.3±0.4 Gt yr^1 from 2007 to 2008 [Rignot et al., 2011]. Besides that, there are differences in the SMB throughout the ice shelf. The SMB is negative near the grounding line, while the SMB becomes positive when moving more southwards, due to a decrease in evaporation, wind erosion and sublimation as a result of the kadiabatic winds [Horwath et al., 2006]. Since the SMB is negative around the grounding zone, there is a sufficient amount of surface melt to form supraglacial lakes during the summer months [Kingslake et al., 2015]. Near the grounding zone, summer surface melting is sufficient to form supraglacial lakes [Kingslake et al., 2015]. Owing to the potential presence of the supraglacial lakes, streams might sporadically drain through. The shelf, therefore, is possibly vulnerable to hydrofracturing [Lenaerts et al., 2017] and thus interesting for further research.

3.2 Data

In this section, a description will be given of the data that were used in this study, namely Sentinel-1, Sentinel-2 and Regional Climate Atmospheric Model data. The Sentinel-1 and Sentinel-2 missions are both parts of the Copernicus Programme from the European Space Agency (ESA). These satellites have their own mission objectives and spatial products. The Regional Climate Model

3.2.1 Sentinel-1

The Sentinel-1 mission is a constellation of two equivalent radar imagery satellites in the same orbit. Sentinel-1A was launched on 3 April 2014 and Sentinel-1B on 25 April 2016 from a Soyuz rocket from Europe's Spaceport in French Guiana. The mission is designed to constantly provide data and information products of areas on land, which can be used for climate change and hazard-related purposes [Torres et al., 2012].

The orbit of the Sentinel-1 mission is sun-synchronous, near-polar, and circular at a height of 693 km with an inclination of 98.18°, the cycle is repeated every 12 days and has 175 orbits per cycle. The ground-range resolution of Sentinel 1 is up to approximately 5 x 20 meters for IW swath. The resolution is swath-depended, in this research this comes down to 10 meters. The satellites are creating C-band synthetic aperture radar images, which are independent of weather and time conditions [Torres et al., 2012].

The constellation of the two satellites has four different operational modes, which differ in polarization, spatial resolution, and swath width: Strip Map (SM), Interferometric Wide Swath (IW), Extra Wide Swath (EW), and Wave (WV). The Sentinel-1 program provides four different data products: the raw level 0 data, the processed level 1 Single Look Complex (SLC) data, Ground Range Detected (GRD) level 1 data, and level 2 Ocean (OCN) data [Torres et al., 2012].

In this study, Sentinal-1 data that is used is in GRD format and IW swath mode results in the data products at a spatial resolution of 10 meters and has HH polarization [Dirscherl et al., 2021a]. All data is acquired over the period from 1 November to 31 March from 2016-2021.

3.2.2 Sentinel-2

The Sentinel-2 mission is a constellation with two identical satellites which fly in the same orbit but are phased 180 degrees. The Sentinel-2A was launched on 23 June 2015 and Sentinel-1B on 25 April 2016 from a Vega rocket from Kourou, French Guiana. The mission objective is to provide consistent global high-resolution, multispectral images on a frequent basis [Gascon et al., 2014].

The Sentinel-2 mission delivers multi-spectral data with 13 different bands. These bands are as already described in the visible, near-infrared, and short wave infrared parts of the spectrum. The orbit of the Sentinel-2 satellites is sun-synchronous at a height of 786 km with a 10:30 a.m. descending node, the cycle is repeated every ten days and has 14.3 rotations per day. Depending on the band the spatial resolution is 10, 20, or 60 meters with a swath width of 250 kilometers [Gascon et al., 2014].

The Sentinel-2 mission provides two main data products: level 1-C and level-2A. The first is the top-of-atmosphere reflectances, while the latter are surface reflectances [Gascon et al., 2014].

For this research the Sentinel-2 data is filtered with a scene cloud cover of less than 75 % and is within the time frame of 1 November and 31 March over the years 2016 to 2021. The presence of the clouds will make the scenes not functional.

3.2.3 Regional Climate data

To study the water volumes of the Nivlisen ice shelf using a Regional Climate Atmospheric Model, data from RACMO is used. In this research the parameters of snowmelt, refreezing, precipitation, and snowfall are implemented in the calculations. The data provided by RACMO has a spatial resolution of 27 kilometers and a daily temporal resolution over the melt seasons from 2016 through 2021. Each parameter contains a flux of the relevant quantity in $kg\ m^{-2}\ s^{-1}$.

3.3 Reference data

The reference data is used to support the different methods. A digital elevation model provides the height of the ice shelf, while a velocity model presents the ice flow of the shelf.

3.3.1 Digital Elevation Model

Understanding the topography of the ice shelf and surrounding area contributes to understanding the origin of the supraglacial lakes. The topography is described by the Reference Elevation Model of Antarctica (REMA). The REMA has a resolution of 8 meters and the data is divided into tiles of 100 by 100 kilometers, so-called strips. These strips contain the elevation, a timestamp, and an error estimate [Howat et al., 2019]. During this research, the elevation and timestamp are used to calculate the elevation model at the desired date. The tiles that contain the correct information are: `52_34`, `52_35`, `53_34`, and `53_35`. In figure 3.3.12 these tiles are shown, the elevation according to the REMA given in meters (figure 3.3.13a) and the moment of acquisition of the elevation given in days since 2000-01-01 UTC. (figure 3.3.13b).

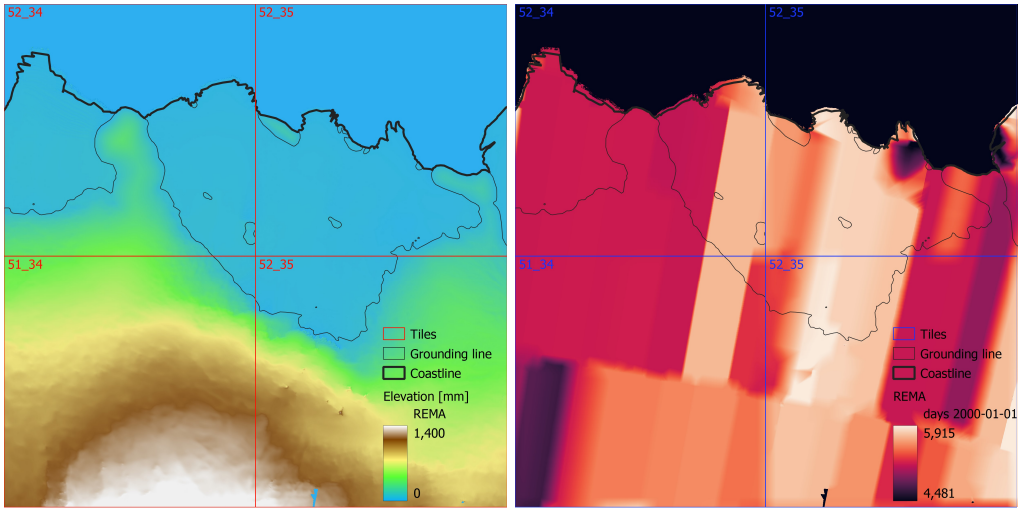

(a) (b)

Figure 3.3.12: The elevation around Nivlisen (a) and the date of the acquisition (b). The different tiles, the grounding line and the coastline are highlighted in both images

3.3.2 Velocity model

As mentioned in previous sections, the ice on Antarctica and its associated ice shelves are flowing. These movements change the topography therefore requiring the REMA to be corrected accordingly. The speed of ice is given in a velocity model which is given in $mm\ yr^{-1}$ and has a spatial resolution of 120 meters.

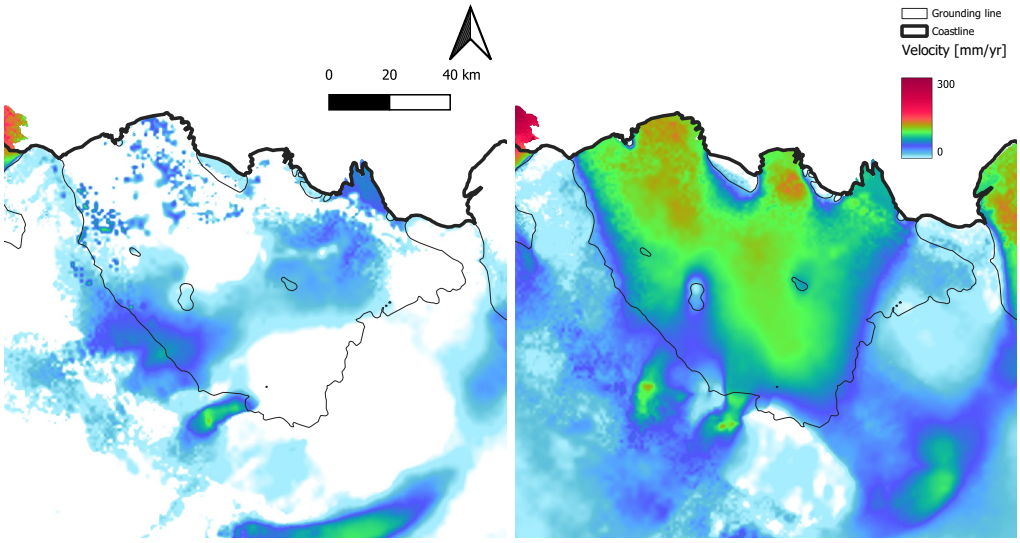

(a) (b)

Figure 3.3.13: Velocity model according of Nivlisen and its surroundings to `https://nsidc.org/apps/itslive/` in mm per year, grounding line and coastline are visualized

4 Methodology

The upcoming chapter explains how the water extents, depths, and volumes for each respective lake were calculated in this study, using satellite observations, a digital elevation model, and data from a climate model.

4.1 General workflow

The research consists of three main parts that come together in a comparison between these approaches and allow the research questions to be answered. Three different methods were used to determine the volume of the supraglacial lakes at Nivlisen from 2015 - 2021. The methods in question are the following:

i. Reflectance method using S2 lake mask;

ii. Kernel method using S1S2 lake mask;

iii. RACMO climate data using Pysheds;

Methods 1 and 2 were based on satellite images and method 3 was based on data from the climate model RACMO. The satellite-based methods made use of lake masks. A lake mask is a raster layer; the pixels containing water are assigned a value of 1, and the others are assigned a value of 0. The S2 lake mask (method 1) used only Sentinel-2 images, whereas the S1S2 lake mask (method 2) also used Sentinel-1 images. The reflectance method, used in method 1, calculates the depth using different bandwidths per pixel. If both a DEM and lake mask were available, the kernel method could be used to estimate the depth per pixel, as done in method 2. By using parameters given by RACMO, such as melt, refreeze, rain, and snowfall, the volume of meltwater is known. It then became possible to run this volume of water tthrough a hydrological model to see where the water accumulated, as done in method 3. In table 1 an overview is shown of the methods using the different calculations for area, depth, and volume.

When calculating volumes, there are two steps in which differences can be obtained, namely the determination of area and depth. In this thesis, the methods are also distinguished in this way. The ways in whixch area, depth, and volume are calculated are discussed in the sections **??**, **??** and **??**. The different outcomes of these methods will be compared in the result section in the same order.

#	**Area determination**	**Depth retrieval**	**Volume calculation**
1	S2 Lake mask	Reflectance method	Area times depth
2	S1S2 Lake mask	Kernel method	Area times depth
3	Hydrological model	Hydrological model	RACMO

Table 1: The three methods that are used in this research for a comparison of area, depth and volume of the supraglacial lakes on Nivlisen Ice Shelve.

The general workflow of the three different methods is given in figure 4.1.14. The three different methods are indicated in the three boxes in different colors. The cones indicate data, the square boxes indicate the type of technique, and the rounded rectangle represents the final products of each technique. In the middle is a fifth box that indicates what the methods are compared to area, depth and volume.

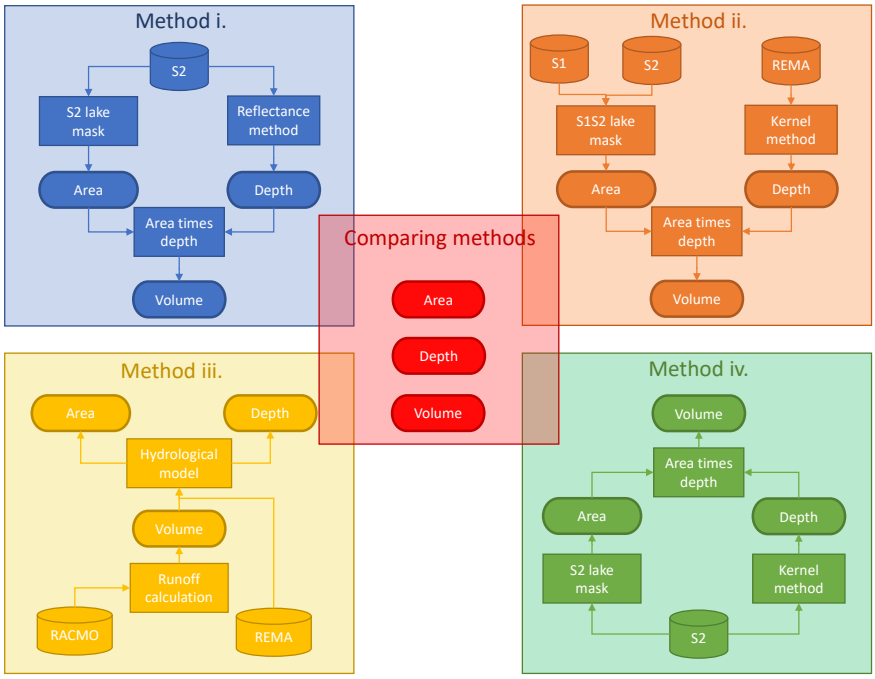

Figure 4.1.14: General workflow of the four different methods with their techniques for determining the area, depth, and volume of the melting ponds in each box and a separate box for comparing the outcomes.

4.2 REMA displacement

The kernel method (method 2: depth retrieval) and the hydrological model (method 3: area determination and depth retrieval) made use of REMA data. The elevation constantly changes due to the fact that ice is flowing. For this reason, it is important to calculate the corrected elevation at the desired time, equal to the time of the satellite or model data of the partical technique.

Determining the corrected elevation is based on a number of steps (figure 4.2.15). The method used satellite or RACMO data at a given date. In the REMA data, the time when the height was acquired is also indicated. This allowed the difference in time between the REMA and the technique to be determined. The velocity model is given in x and y and in combination with the time the displacement can be determined in the x and y direction. Then the corrected elevation at the desired time was computed by using the calculated displacement with the *displace* function in GEE over the original elevation. A result of the workflow is shown

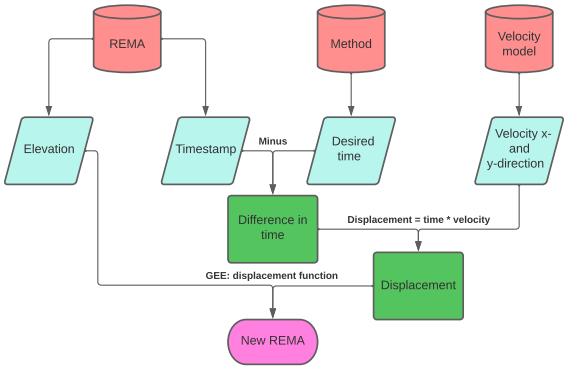

Figure 4.2.15: Workflow for constructing displaced REMA.

(figure 4.2.16). It can be observed that the changed REMA looks more realistic since the water is located in the lower elevated pixel. A possible limitation of the S1S2 lake mask is that the exact date is not known, therefore the middle date of the biweek was used. This may have an impact in the case of a sharp transition in elevation, but is likely to remain limited. In the case of RACMO data, the exact date was known and could be calculated more accurately. In addition, the velocity model is an average over the last 10+ years and so will also have some limitations.

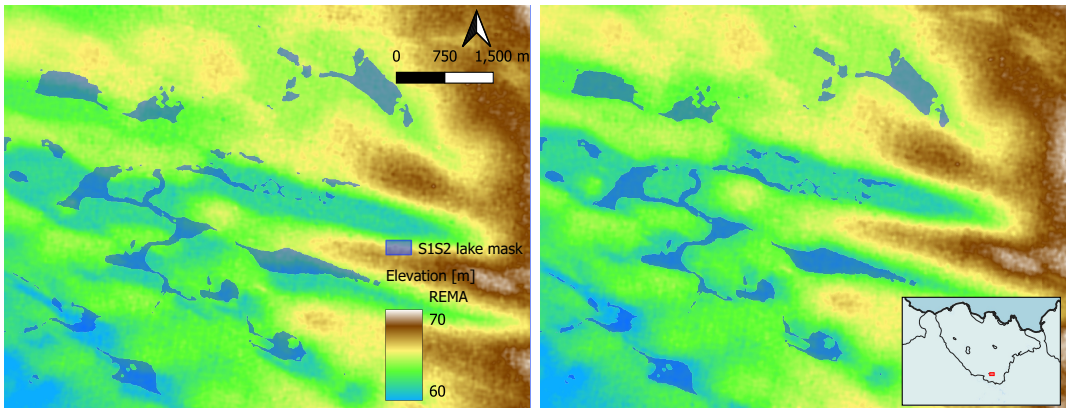

(a) (b)

Figure 4.2.16: The original (a) and displaced (b) REMA 2020-01-08 and the S1S2 lake mask of the first biweek of January 2018

4.3 Method 1

Kort uitleggen hoe deze methode werkt met alle stappen er bij en evt. een flowchart van de methode. Uitgebreider dan eerst gegeven is.

4.3.1 Area determination

The S2 lake mask was calculated according to a threshold-based classification algorithm using Sentinel-2 images. The algorithm was developed by Mousavi [Moussavi et al., 2020] and was validated resulting in overall accuracies of $> 95\%$ for Landsat-8 and $> 97\%$ for Sentinel-2. Lakes, clouds, and rocks were distinguished based on optical data. The data was pre-processed in this study by filtering the scenes that contain clouds of more than 0, 25, 50 and 75 percent. Next, A sensitivity analysis was done on the influence of clouds in detecting lakes by comparing the water extents for the different filter thresholds. Finally, the images with cloud cover less than 25 % were used to determine depth and volume. The S1S2 lake mask made use of the same threshold value, therefore the comparison was under the same circumstances. In particular, the pixels containing liquid water were classified based on the Normalized Difference Water Index (NDWI) value (see formula 5), in which the blue and red band represent Sentinels-2's Band and Band 2, respectively [Moussavi et al., 2020].

$$NDWI = \frac{Blue - Red}{Blue + Red} \tag{5}$$

To be able to differentiate between the clouds and rocks, the Normalized Difference Snow Index was determined, as displayed in equation 6. For Sentinel-2 images, B3 and B11 represent the green band and the shortwave infrared, respectively [Moussavi et al., 2020].

$$NDSI = \frac{Green - SWIR}{Green + SWIR} \tag{6}$$

Subsequently well-balanced training set was chosen, containing different study sites consisting of manually chosen areas such as lakes, slush, snow, shaded snow, sunlit rocks, shaded rocks, clouds, and cloud shadows [Moussavi et al., 2020]. For each pixel within the training set, the values of the useful bands and the calculated indices were given and a class was assigned. The resulting pixel distributions are shown in figure 4.3.17. Based on analyzing the distribution of the pixel values of these classes, thresholds are chosen (see table 2) [Moussavi et al., 2020]. Furthermore, the threshold values chosen by Moussavi et al (2020), were also used in this study to create a lake mask. An overview of mask generation is shown in figure 4.3.18.

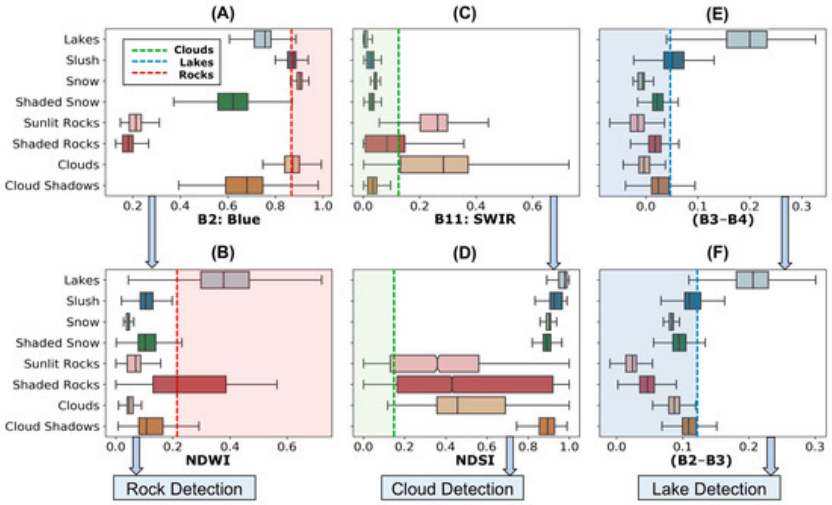

Figure 4.3.17: The distribution of pixel values represents different properties of lakes, slush, snow, shaded snow, sunlit rocks, and shaded rocks, clouds, and cloud shadows, [Moussavi et al., 2020]

The area of each pixel is given by the Sentinel-2 data. The total area of water can be determined by adding

Index	Name	Threshold
NDSI	Normalized Difference Snow Index	0.85
NDWI	Normalized Difference Water Index	0.3
B3-B4	Difference green and red	0.09
B2	Blue	0.4
B10	Short Wave Infrared	0.01
B11	Short Wave Infrared	0.1

Table 2: The calculated threshold for each index based on the pixel distributions

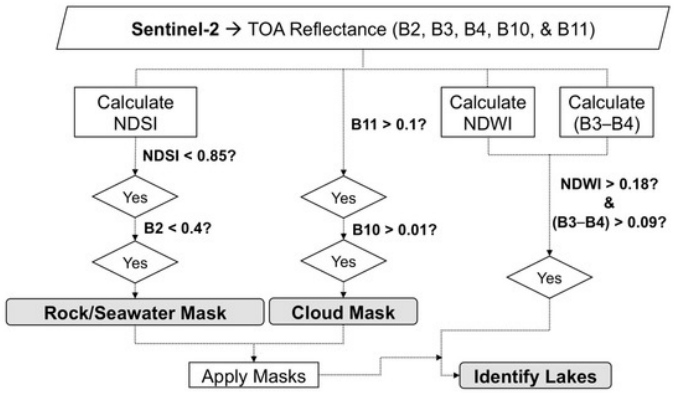

Figure 4.3.18: Workflow lake mask generation, [Dirscherl et al., 2021b].

all the pixels in the mask and multiplying by the pixel area, as shown in equation 7. In the equation, A_{water}, A_{Pixel} and n_{Pixel} are the total water extent, the pixel area, and the number of pixels that are containing water, respectively.

$$A_{\text{Water}} = A_{\text{Pixel}} \sum_{i=1}^{n} n_{Pixel} \tag{7}$$

Classification using solely Sentinel-2, several problems were expected to potentially arise. Firstly, the low temporal resolution in comparison to the number of possible melting days (days during the Austral summer), as there was an average overpass of three times a month. Due to filtering of the scenes with more than 75 percent cloud cover, the actual temporal resolution was lower (mostly twice a month). In addition, the presence of clouds could result in a possible unusable image, as clouds cannot be penetrated by Sentinel-2. Secondly, the presence of clouds, which could cause miss-classification, as shown in figure 4.3.17, the shadows of clouds could be misclassified as water. The figure also shows that the shadow of rocks could cause a problem. Thirdly, water beneath clouds was not accurately visible and therefore could not be properly classified. Lastly, a problem that could arise from using an optical satellite, is that it could not penetrate trough ice. A possible situation where that would cause a problem, is when the top of a water volume refreezes, wwhile there is still liquid water present underneath. Subsequently, the pixel would be be classified as non-liquid and therefore would not be taken into account for the final volume calculation. One could argue that it should be classified as water since there is water underneath. Therefore the water extent will eventually be smaller, as will the water volume.

4.3.2 Depth retrieval

The reflectance method is based on the principle that light passing through water is influenced by the amount of water. The light is scattered of absorbed by the water column. The calculation of the lake depths is based on recent studies of supraglacial lakes on Greenland [Philpot, 1989]. The equation to derive the lake depth

from optical satellite images is formulated as follows:

$$z = \frac{ln\left(A_d - R_\infty\right) - ln\left(R_w - R_\infty\right)}{g} \tag{8}$$

where z is the lake depth, A_d is the lake bed's albedo, R_∞ and R_w are the reflectance of deep water (depth ¿ 40 meters) and the observed water, respectively, and g is the two-way attenuation coefficient [Philpot, 1989]. It is called two-way because it covers the presence of absorption and scattering processes as well in the upward as in the downward pathways. A_d, R_∞ and g are influenced by the wavelength and so which band were used. Longer wavelengths are more applicable to small depths and lower wavelengths and vice versa. Since the lake depths are relatively small (less, a longer wavelength is used, B4, less than 4 meters. According to Moussavi et al. 2020, the parameters are derived for Landsat 8 and Sentinel-2, in this thesis, only the parameters for S2 are calculated and used, since only S2 scenes are used. A_d was determined by averaging three pixels outside the lake to reduce the possible error of the classification [Moussavi et al., 2020]. According to Williamson et al, an appropriate value for g is 0.83 [Williamson et al., 2018]. For each image, the reflection of deep water pixels for the red band is determined, the median of which is the value for R_∞. For this, Moussavi et al. 2021 used 12321 images from 2016 to 2019 containing the only images without clouds (see figure 4.3.19). Using this, the R_∞ was determined to be 0.04.

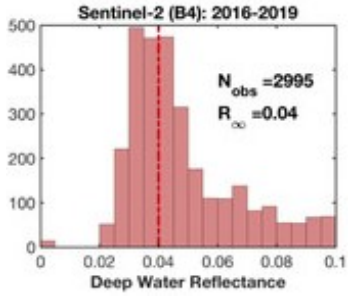

Figure 4.3.19: Distribution of the R_{infty} values derived from the different Sentinel-2 images, the meridian of R_{infty} is determined on 0.04, [Moussavi et al., 2020]

Now the parameters are known, the depth per pixel can be determined executing equation 8. However, it is not possible to calculate the depth of very large lakes with ten meters resolution. In GEE the function *reduceconnectedcomponents* is used to calculate A_d, it applies a reducer (mean) over pixels that are connected and thus are considered to be one waterbody. The function can handle a maximum number of pixels, 1054. In order to be able to calculate the depths, a scale of 70 was chosen for these lakes, so that they can be calculated. The water extent of a lake A mosaic was then made of the depths at 10 m resolution and the missing pieces at 70 m resolution. Due to the fact that the resolution is coarser the edges of the lakes will be deeper and sharper transition between pixels in comparison to the 10-meter resolution. Generally the coarser resolution will lead to an overestimation in comparison to the finer resolution.

4.3.3 Volume calculation

For methods 1,2 and 4, the depths have already been calculated in the earlier section. The area of each pixel is known and this makes it possible to calculate the volume. The total water volume can be calculated by multiplying the sum of the depths by the surface area of the water [Moussavi et al., 2020]:

$$V_{\text{lake}} = A_{\text{Pixel}} \sum_{i=1}^{n} d_i \tag{9}$$

where V_{lake} is the water volume, A_{Pixel} is the area of the pixels within the water extent, and d_i is the lake depths per pixel.

4.4 Method 2

Kort uitleggen hoe deze methode werkt met alle stappen er bij en evt. een flowchart van de methode. Uitgebreider dan eerst gegeven is.

4.4.1 Area determination

The S1S2 lake mask is acquired from Dirscherl and makes usage of Sentinel-1 and Sentinel-2 satellite imagery. Eventually, both classifications are merged, and a maximum lake extent is created by making a mosaic of all the classification maps of Sentinel-1 and Sentinel-2 every two weeks during the melt season [Dirscherl et al., 2021b]. Dirscherl et al. 2021 created the bi-weekly mask extents for the Nivlisen Ice Shelf, these are used to calculate the water extents. Below is a brief description of how Dirscherl et al. 2021 did this.

The Sentinel-1 data is pre-processed using SNAP, including orbit correction, thermal noise removal, radiometric calibration, speckle filtering, and terrain correction [Dirscherl et al., 2021a].
A convolutional neural network (CNN) based on a residual U-net is used to calculate the melt water extents in the Sentinel-1 images. Due to the fact that meltwater lakes and other features like blue ice, shadows, and wet snow are similar looking in SAR imagery and due to wind roughening and speckle noise, utilizing a deep learning network is preferred over a regular technique [Dirscherl et al., 2021a]. The outcome of the method was then tested on 23,000 random points spread over 10 independent test sites. An F1 score of 93 percent was calculated across these regions (Baumhoer et., 2021). The misclassifications are generally caused by radar shadow, wet snow, and blue ice.

The classification approach for the Sentinel-2 imaginary is a machine learning algorithm, a random forest classifier. Only the Sentinel-2 images which have less than 75% cloud cover are selected. As with the S2 lake mask, different indices are calculated over a dataset. These differ from those of the S2 lake mask, in addition, now only rock, shadow, snow/ice, and water are distinguished.The random forest classifier is trained on a high-performance computing cluster with designated spectral bands over different regions of Antarctica. The labels are created manually and the topographic variables are derived from the Antarctic TanDEM-X [Dirscherl et al., 2020]. Both Sentinel-1 and Sentinel-2 classifications are post-classified with bands, indices, morphological erosion, and topographic and coastline masking.

The resolution of the Sentinel-1 and Sentinel-2 data are both 10 meters. The total water area extent can be derived in a similar way as in the section Area determination using equation 7.

4.4.2 Depth retrieval

The kernel method is an algorithm to calculate the depth of a lake from a DEM and a lake mask. Problems for using optical satellite data is that the scenes can be disrupted or even unusable due to the presence of clouds. Using e.q. InSAR data (SMISS) is independent of clouds and is have a better temporal resolution. Therefore it is beneficial to develop a method that is not based on optical satellite data and in this spirit, the kernel method was produced. The method is based on two principles. It follows the idea that the water level is horizontal and the idea that the highest situated point where water is indicated as the top of the water table. The input for this method is only a DEM and a lake mask which outputs the depth per pixel.

In figure 4.4.20 is the procedure of the method outlined. At first, an image is made of each different lake of a single lake mask, together as an image collection. Then that image collection is multiplied by the REMA, the result is the elevation of each pixel that contains meltwater. Then, for each lake (each image), a moving window passes over it, varying in size. A sensitivity study was performed to determine the influence of the different kernel sizes. Three sizes are chosen: 250, 500 and 1000m and later analysed in the results section. The ice shelf has a slope as well and this slope affects the elevation, so over The kernel has to be smaller for smaller lakes, and larger for the larger ones vice versa. Each time, from each kernel square the highest pixel pixel is selected to be the top of the water table of that same square. To avoid outliers, the 95th percentile is chosen. The values that become negative (5th percentile) will be set to zero. Since the water level is horizontal, the highest point means the top of the water level. Then the height of each water pixel is

subtracted from the maximum height in the kernel, the water depth per pixel.

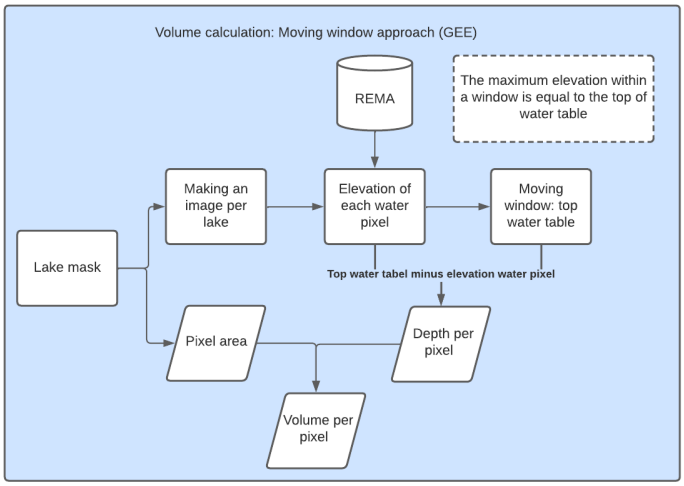

Figure 4.4.20: Workflow of the kernel method.

Determining the depth using the kernel method in study has three possible problems. First, the size of the window is not optimal. Second, the mask is not completely accurate, see section Area determination. If one or more pixels are wrongly classified as non-water, while they are the highest within the kernel, all the depths of those pixels in the window are underestimated. In particular, the presence of ice lids affects this, as they are often formed where it is shallower and thus higher. Finally, the DEM is not quite corrected. This is because the velocity model has a lower resolution, 120 meters versus 10 meters, and it is an average over 10 years, see section REMA displacement. In addition, there is no exact date of the mask because it uses a biweekly extent. If the DEM is wrong, it changes the final depth, see section above.

4.4.3 Volume Calculation: Area times volume

Calculating the volume is done in the same way as method 1, Volume calculation. The depths per pixel are multiplied by the pixel areas.

4.5 Method 3

Kort uitleggen hoe deze methode werkt met alle stappen er bij en evt. een flowchart van de methode. Uitgebreider dan eerst gegeven is. Voordelen regional climate model: hogere temporele resolutie en "in de toekomst kijken", nadeel coarse spatial resolutie

4.5.1 Volume Calculation

Unlike the satellite-based methods, the climate model-based method first calculates the volume of water and then the areas and depths. As described earlier, RACMO calculates melt, refreezing, precipitation, and snowfall over a tile of 27 kilometers per day. First, the fluxes of the relevant parameters are converted into millimeters per day, as described in equation 10.

$$p_{day} = \frac{p_{flux} s_{day}}{\rho_{water}} 10^3 \tag{10}$$

, where p stands for parameter, s_{day} means seconds per day which is 86,600 seconds and ρ_{water} is the density of water 997 kgm^{-3}. After this step, it is known for each parameter per location how many millimeters are added or subtracted per day. Then the integral is taken over time. The start time is chosen as the first day of that year's melting season, and the end time is the desired day when one wants to know the runoff. Then the runoff can be calculated per tile, using formula 12. Precipitation is the sum of rain and snowfall, since rain is not a calculated parameter precipitation is subtracted from snowfall. During the day the temperature

is higher than during the night, in addition, refreezing does not take place when it melts and vice versa. Therefore, on the day of calculation, refreezing is not included.

$$Runoff = Snowmelt - Refreezing + Rain \tag{11}$$
$$= Snowmelt - Refreezing + (Precipitation - Snowfall) \tag{12}$$

Using formula 12 to calculate the runoff per tile, is shown in figure 4.5.21. Lastly, the runoff was summed over all pixels within the catchment to obtain the total amount of net modeled meltwater. The snowmelt computed by satellite is calculated over a biweekly max extent, in order to compare as fairly as possible a biweekly max is chosen for the RACMO data as well. The maximum value of the weeks is chosen to be the estimated volume. The total volumes derived by RACMO will be compared to the volumes calculated by the other methods in the result section.

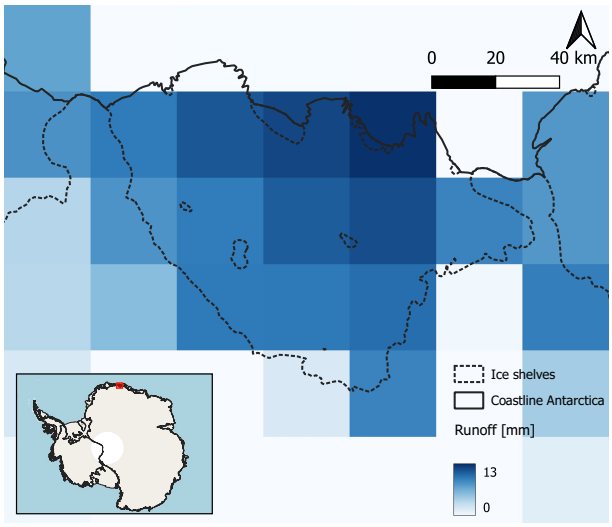

Figure 4.5.21: RACMO image 2019-01-01

4.5.2 Area determination

The total volume has already been calculated using RACMO, see section Volume Calculation. However, a vulnerability analysis requires the water volume per lake. In addition, it provides an opportunity to compare the depths and surfaces of the supraglacial lakes to gain further insight into the method. For this reason, it is necessary to determine where the calculated water (runoff) is transported to and accumulates. A hydrological model can provide the answer to this and the he python module *pysheds* makes it possible to do this flooding experiment. The module contains the function *Rapid flood Spilling Method* (RFSM), which fills the DEM with water and calculates in which direction the water flows based on the DEM. The amount of water can be adjusted and is in the form of dataframe. The calculated runoff, section Volume Calculation, can be used as input.

The day when the most runoff of the biweek is estimated is chosen and with the net runoff and the elevation, the water extent can be estimated. It is important to use the REMA without depressions or sinks, this is done using the functions *fill_depressions* and *resolve_flats* of the Pysheds module. Otherwise, all the water will accumulate in the cells that have no drainage value. A sink is a cell that does not have an associated drainage value. Drainage values indicate the direction that water will flow out of the cell, and are assigned during the process of creating a flow direction grid for the landscape. The resulting drainage network depends on finding the 'flow path' of every cell in the grid, so it is important that the fill step is performed prior to creating a flow direction grid. Then the water, calculated using RACMO, is spread over the adjusted elevation model. The runoff data is downscaled to the desired resolution, 500 meters. Then

the (RFSM) is executed to determine where the water eventually accumulates. This results is a data frame consisting of the elevation of the water pixels. Then a 3D model of where the water accumulates can be made in python using the DEM (grey) and waterlevel (cyan) values are already calculated, an example can be found in figure 4.5.22. In this image, one can obtain where the water accumulated. Finally, it is possible to calculate the total area via formula 7, by multiplying the number of pixels by the pixel size.

There are three complications that could occur while using pysheds. First, the area of Nivlisen is too large to run the RFSM in the desired resolution of 10 meters due to computational costs. A coarser resolution therefore should be used, 500 m. Second, the pysheds module is developed for an endorheic catchment, having no outlet, while the Nivlisen Ice Shelf is an exoreic catchment since the South Ocean is the outlet. This can be solved due to clipping the REMA and removing manually the water that would flow into the sea. Three, the algorithm injects the water at the lowest point, instead of pouring it over the area, resulting in one water body at the same elevation.

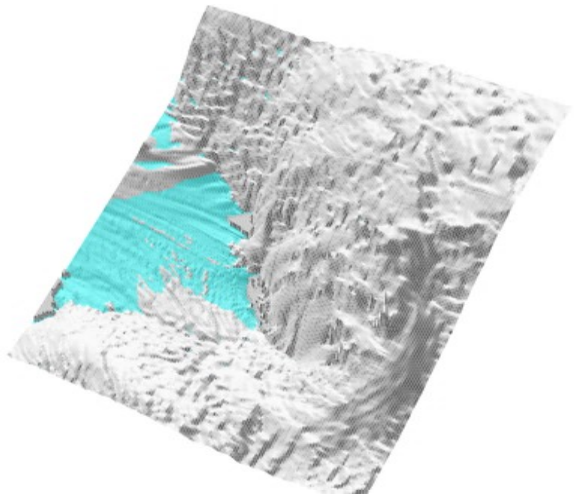

Figure 4.5.22: 3D representation of water flood from RACMO data using RFSM

4.5.3 Depth retrieval

To obtain the depth of the supraglacial lakes for the climate-based method only one step has to be executed. As already described in section **??**, a data frame consisting of the elevation of the water pixels is derived. To obtain the depth per pixel, the elevation according to the REMA is subtracted from the elevation of the water pixels. In the results section, these will be compared to the satellite-based methods. However, it makes it difficult that the resolution of satellite-based methods is 10 meters whereas the resolution of the model-based method is 500 meters.

5 Results

The results from the analyses of the different methods, as described in the previous chapter, will be discussed in this chapter. The following subsections will each compare the various used methods for determining the area, depth and volume of the meltwater on the Nivlisen Ice Shelf

5.1 Area determination

According to the steps described in section 4, the water extent of the supraglacial lakes was determined. A sensitivity analysis on the S2 lake mask with different filter values for cloud cover was visualized and will be discussed in section 5.1.1. The different methods and their respective results for the water areas are compared in section 5.1.2. Also, the respective differences and similarities will highlighted.

5.1.1 Sensitivity Analysis: Cloud cover S2 lake

To demonstrate the influence of the presence of clouds on the S2 mask, a sensitivity analysis was applied over the Nivlisen Ice Shelf during the period of 2016 to 2021. The S2 images were filtered based on less than 25, 50, 75 and 100 percent cloud coverage, respectively, see figure 5.1.23. The difference in water extent caused by the individual filters is not seasonally related based on this figure, i.e. the chance of a specific cloud percentage in November is not greater or smaller than in January. However, the difference in cloud coverage does influence the amount of water extent for most of the images; only three scenes are not at all affected by presence of clouds (JanB '17, JanA '18, and JanB '18). In general, it was observed that most water could be detected when the presence of clouds was allowed and when the filter was less strict. The lower threshold causes more scenes to be selected and thus increases the chance of detecting water. In addition, it was found by visual inspection that shadows caused by clouds could be misclassified as water. This caused an increased chance of water volume overestimation. However, this wrong classification is small in comparison to the well classified lakes based on visual inspection. For instance, the case of JanB'19 shows clearly visible supraglacial lakes, even though there are many clouds present. Although these clouds are not located above the melting ponds and thus not influence the result. Nevertheless, a part of the scene is removed, as the cloud percentage threshold is not met. Subsequently, the water extent is underestimated. Another example is the case of JanA '19. Here, all scenes have a cloud cover higher than 75%, however, there is still some water visible and the part that is classified correctly. It is obtained that there is even a little underestimation, see figure 5.1.24.

5.1.2 Comparison lake masks

The area was calculated using three different techniques, as mentioned in the methodology, for five consecutive melt seasons (2016-2021). The different biweekly water extents are illustrated in figure 5.1.25 and a table containing the minimum, median, mean and maximum values of the biweekly water extents per melt season (table 3).
As can be observed in the figure and the table, there are three remarkable things. Firstly, for the majority of cases, method 3 overestimates by a factor of 10 in comparison to the methods 1 and 2. When regarding the water extent of method 3 in 3D Looking at the RACMO in 3D and a S2 scene at those specific dates, the suggestion can be made that the overestimation is inaccurate. Secondly, the fact that the S2 lake mask records less water surface area at specific timings. Both methods use the same S2 images and the same cloud threshold, which shows that the S1 part of the S1S2 lake mask has a influence. For example in the case of JanB 2019, there is a part filtered out (see Sensitivity Analysis: Cloud cover S2 lake) for the S2 image, then the S1 component of the S1S2 lake mask causes an larger water extent. The S1S2 mask detects more water in most situations. In some cases, e.g. JanA 2020, it is clear to see that S2 image did not fullfill the cloud cover threshold and thus no water was classified by the S2 mask. Therefore, the S1S2 lake mask, which has the same preprocessing steps, is completely dependent on the S1 images. However, the Sentinel-1 images do not for all cases yield enough to compensate for this difference, JanB 2017 and JanA 2018. Thirdly, it seems the S2 part of the S1S2 lake mask is more strict in classifying water than the S2 lake mask. The differences are mostly around the edges of the lakes. The dissimilarities can have more impact as well, as can be seen in

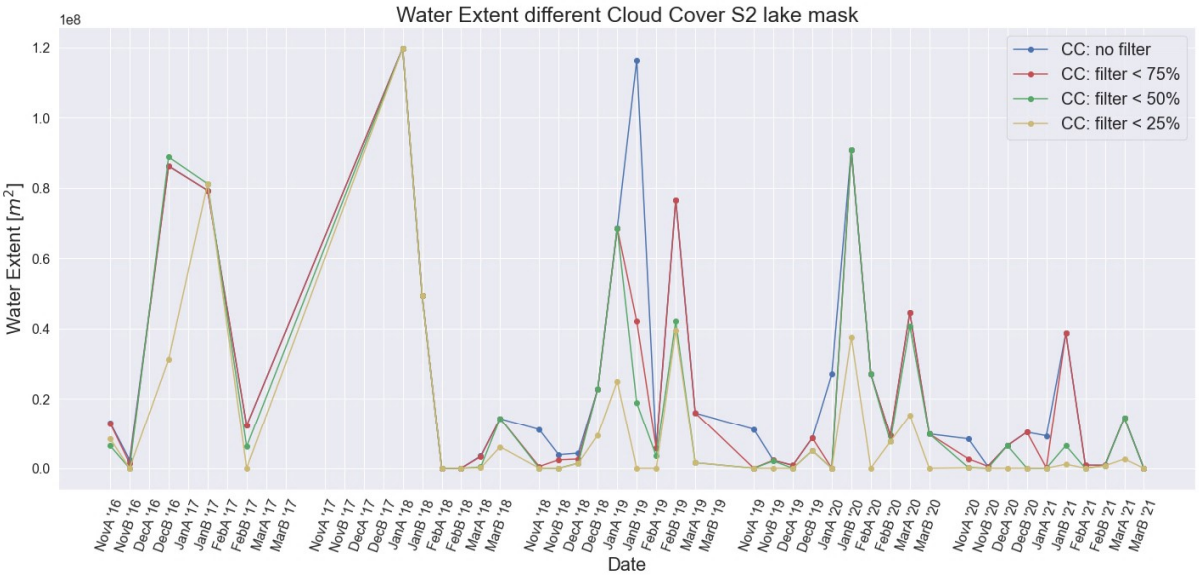

Figure 5.1.23: Water extents on Nivlisen according to S2 lake mask for different cloud coverage

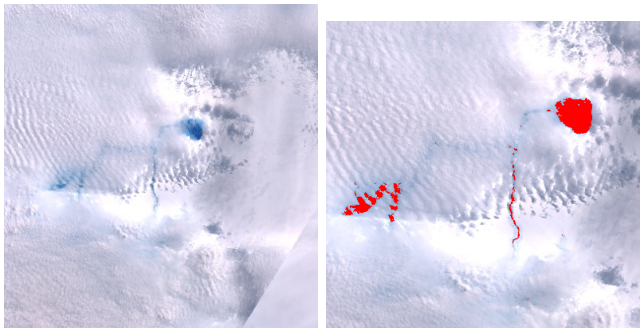

(a) (b)

Figure 5.1.24: CAPTION

figure 5.1.26, which clearly shows both cases. The west part of the image shows relatively large differences in classification, due to a stricter S1S2 mask. On the east, the small differences near the edges are visible where the S2 lake mask estimates a higher water surface.

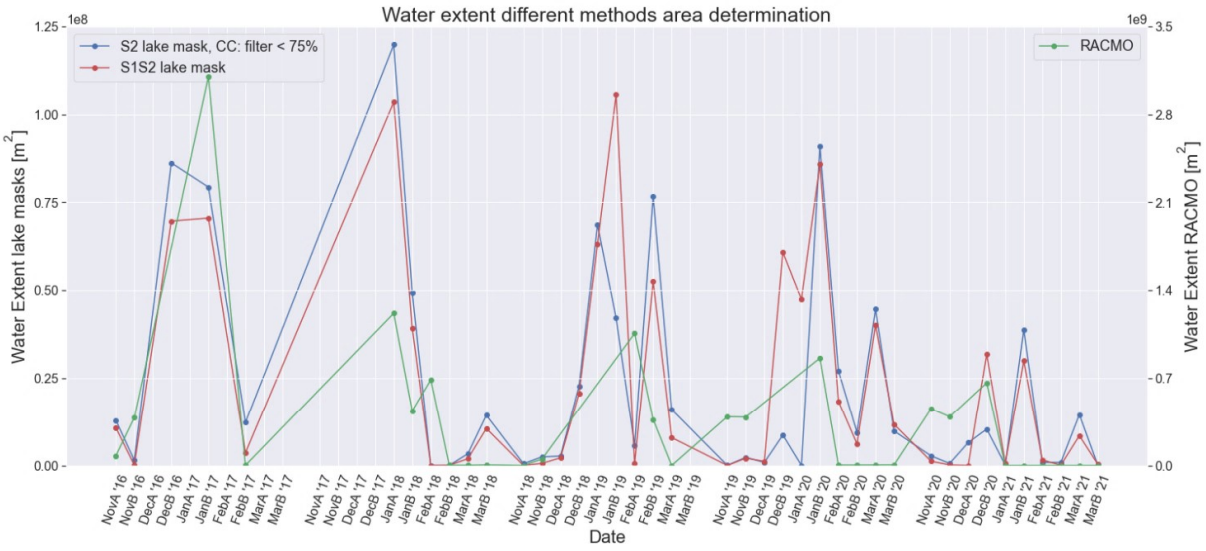

Figure 5.1.25: Water extents on Nivlisen according to S2 lake mask with a cloud coverage of less than 25 % and the S1S2 lake mask

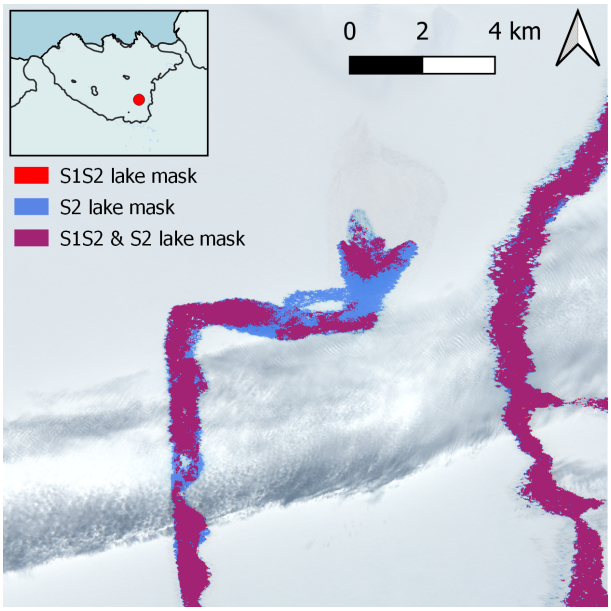

Figure 5.1.26: The S1S2 lake mask and S2 lake mask of JanA 2018 on a satellite image acquired on 12 January 2018.

To strengthen the third point, the surface areas were calculated by juxtaposing the lake masks at the specific times when clouds have little to no influence. In addition, a calculation was done to determine the area size for which the two masks coincide with one another. This was expressed in a percentage for each mask with respect to the other, and attached in figure 5.1.27. It was observed that for the majority of cases, the aerial overlap percentage was higher than 70 %. The previous assumption, namely that the S2 mask is less strict, was hereby confirmed. This can be related to the fact that the percentage of aerial overlap is higher in the S1S2 mask for every case and because there is hardly any influence of clouds. Furthermore, it was observed that for DecB '16 and JanA '19, the overlap percentage was much lower.

	2016-2017			
technique	**min [m²]**	**median [m²]**	**mean [m²]**	**max [m²]**
S2 lake mask	1.456e+06	1.288e+07	3.844e+07	8.623e+07
S1S2 lake mask	1.033e+05	1.075e+07	3.094e+07	7.054e+07
Hydrological model	1.000e+06	2.281e+08	8.894e+08	3.100e+09

	2017-2018			
technique	**min [m²]**	**median [m²]**	**mean [m²]**	**max [m²]**
S2 lake mask	6.297e+03	6.297e+03	6.297e+03	6.297e+03
S1S2 lake mask	0.000e+00	6.210e+06	2.586e+07	1.035e+08
Hydrological model	1.250e+06	2.209e+08	3.914e+08	1.218e+09

	2018-2019			
technique	**min [m²]**	**median [m²]**	**mean [m²]**	**max [m²]**
S2 lake mask	4.885e+05	1.591e+07	2.532e+07	7.667e+07
S1S2 lake mask	0.000e+00	7.930e+06	2.812e+07	1.057e+08
Hydrological model	0.000e+00	5.025e+07	2.946e+08	1.056e+09

	2019-2020			
technique	**min [m²]**	**median [m²]**	**mean [m²]**	**max [m²]**
S2 lake mask	9.982e+01	9.043e+06	1.936e+07	9.086e+07
S1S2 lake mask	0.000e+00	1.500e+07	2.735e+07	8.579e
Hydrological model	3.000e+06	4.250e+06	2.357e+08	8.602e+08

	2020-2021			
technique	**min [m²]**	**median [m²]**	**mean [m²]**	**max [m²]**
S2 lake mask	1.199e+03	1.788e+06	7.465e+06	3.878e+07
S1S2 lake mask	0.000e+00	8.858e+05	7.401e+06	3.179e+07
Hydrological model	0.000e+00	0.000e+00	1.671e+08	6.615e+08

Table 3: caption

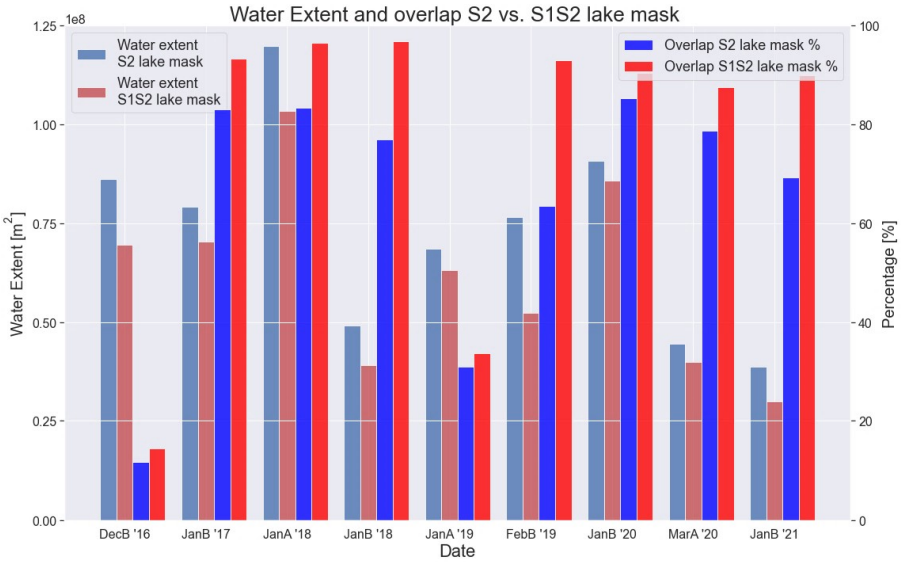

Figure 5.1.27: Caption

Based on studying the true color images and the elevation, it was observed that there were also situations where both satellite techniques possibly come short. Visual inspection showed wrong classifications, caused by shadows of clouds and rocks. This phenomenon occurred for both masks, although more frequently for the S2 lake mask than for the S1S2 lake mask. However, those misclassifications did not influence the result severely. Ice lids (i.e. water with a frozen upper layer) were observed to be wrongly classified on a bigger scale and to be of a larger influence. An example of possible wrong classification due to an ice lid is given in figure 5.1.28. Looking at the Sentinel-2 image, the corresponding masks seems to match well. However, in combination with REMA, it is more likely that it is a larger depression filled with water and there is liquid water underneath the water. The water at the top of the lake is at higher elevations than other parts where no water was observed. Also, the hole in the middle of the lake looks like a frozen ice lid, as it is located at the same elevation and surrounded by water. The Sentinel-1 image does not provide conclusive evidence but is an addition to the presence of an ice lid, the values outside the possibly larger lake are considerably lower than at the lake itself. Hollow circles are seen throughout the entire ice shelf, which are also likely to be ice lids. In the case of the lower part, lakes are clearly visible (figure 5.1.29). However, these are not classified as water by either technique. These lakes are present during most months of the melting season.

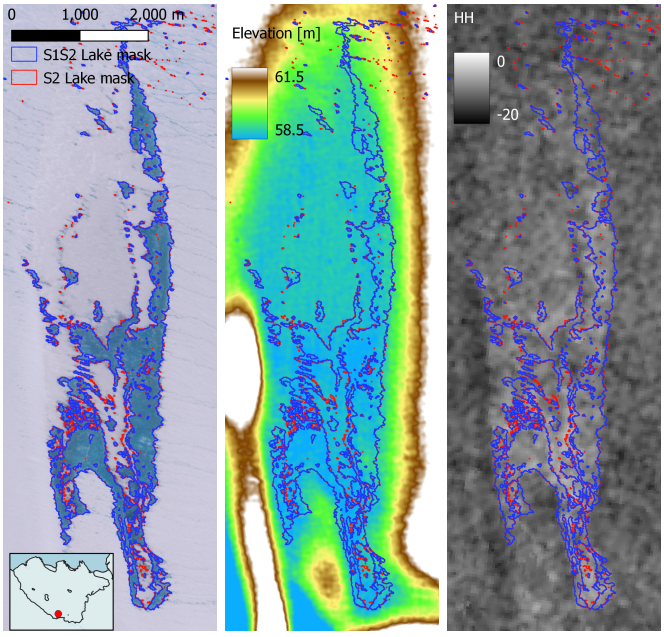

(a) (b) (c)

Figure 5.1.28: Sentinel-2 image, acquired on 12 January 2018 above Nivlisen, in true color (a), elevation according to REMA (b), and Sentinel-1 image, acquired on 10 January 2018 above Nivlisen.

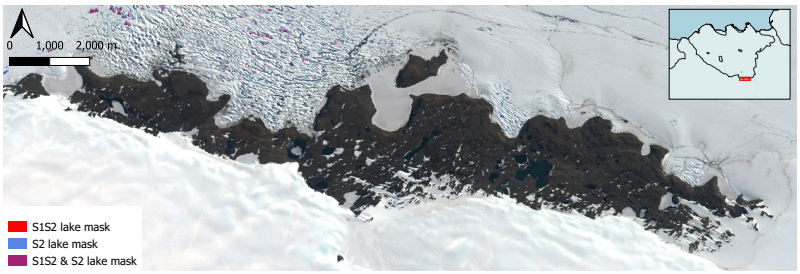

Figure 5.1.29: Sentinel-2 image, acquired on 12 January 2018, and the both lake masks

5.2 Depth retrieval

According to the steps described in section Methodology, the depth of the supraglacial lakes was calculated. In the following paragraphs, a sensitivity analysis on the kernel method with different kernel sizes will be visualized and discussed. Furthermore, the different methods and their corresponding water depths will be compared. Also, the respective differences and similarities will be highlighted.

5.2.1 Sensitivity Analysis: kernel sizes

The different sizes of the windows affect the depths. The depths of the bikweeks were analyzed over time from 2016 to 2021. The radii sizes were 250, 500, and 1000 meters. Some notable examples will be discussed in this section.

In general, it can be said that an increase in kernel size results in greater depths if the lake is larger than the kernel. In case of a small lake, kernel size has no impact. In contrast, it possibly fails for larger sizes in the case of larger lakes. Figure **??** shows the S2 image in true color, the corrected elevation, the depths following the different kernel sizes, and a cross-section of the depths are given in figure **??**. The transect that is drawn is in the direction from north west to south west. One can obtain that the depths calculated with a kernel radius of 250m naturally increase towards the middle of the lake and then decrease again. Looking at the REMA, a similar pattern is observed. In the cases of the other 500m and 1000m kernel radii, it rises up to the middle and then even rises. Looking at the REMA, you see a similar pattern. Due to the size of the lake (width less than 1000m) and the sizes of the kernels the depths calculated by 500m and 1000m are exactly the same.

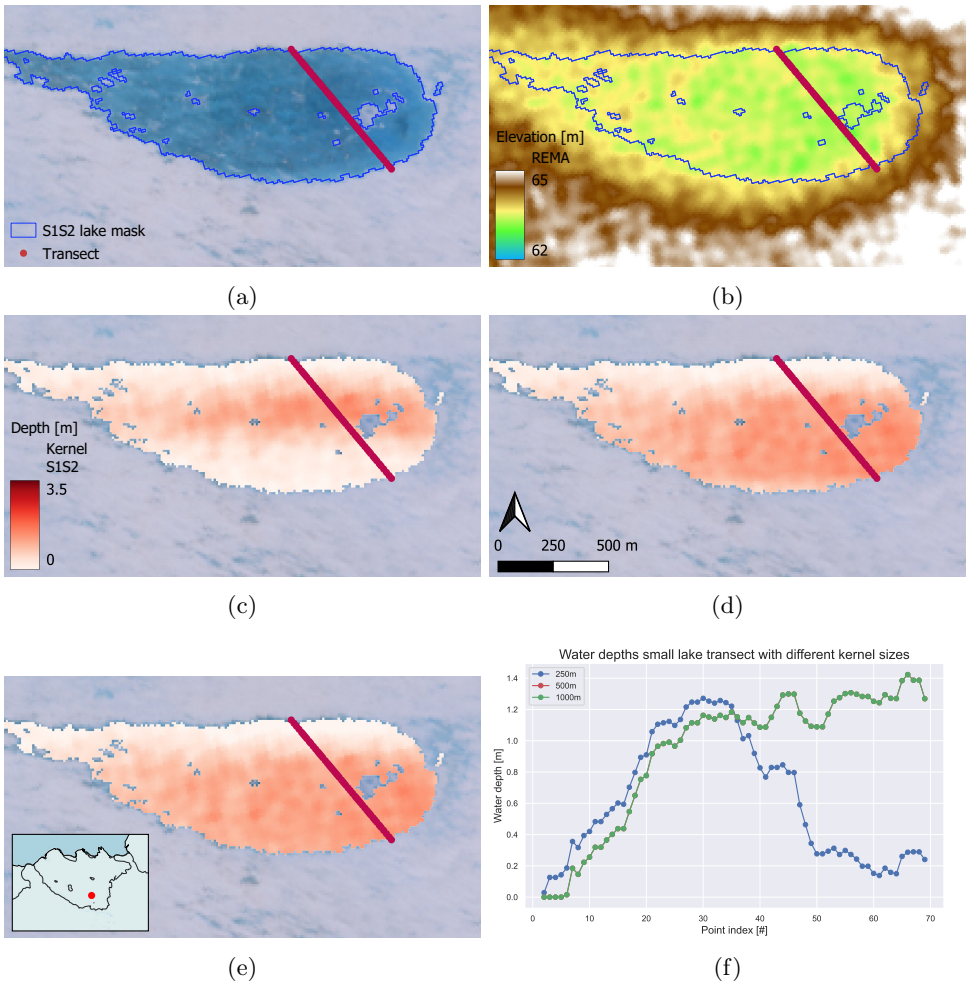

Figure 5.2.30: Sentinel-2 image, acquired on 21 January 2017 above Nivlisen, in true color (a), elevation according to REMA (b), the depths accoring kernel size 250 (c), 500 (d) and 1000m (e), results of the transect from northwest to southeast (f).

Figure 5.2.31 shows a second example of two connected oblong lakes. Again, the satellite image, the REMA, the depths of different kernel sizes, and a cross-section are compared. The transect is drawn from south to north. It can be seen from the REMA that the part in the south is approximately 8 meters higher than in the north. The kernel method is calculated using the elevation, so a steeper slope causes greater depths. It is remarkable that all three follow the same pattern. The fact that the depths decrease around point 2200 and increase towards the south and the north, indicates that two lakes are connected. One can obtain that the depths increase with a larger kernel size. The bigger the depths, the greater the increases in case of a larger kernel size. The 1000m kernel has many 3-meter plus depths, which are unrealistic. It is also visible that in the north (point 0) the 500m and 1000m do not decrease to zero, however this holds for the 250m and looks natural.

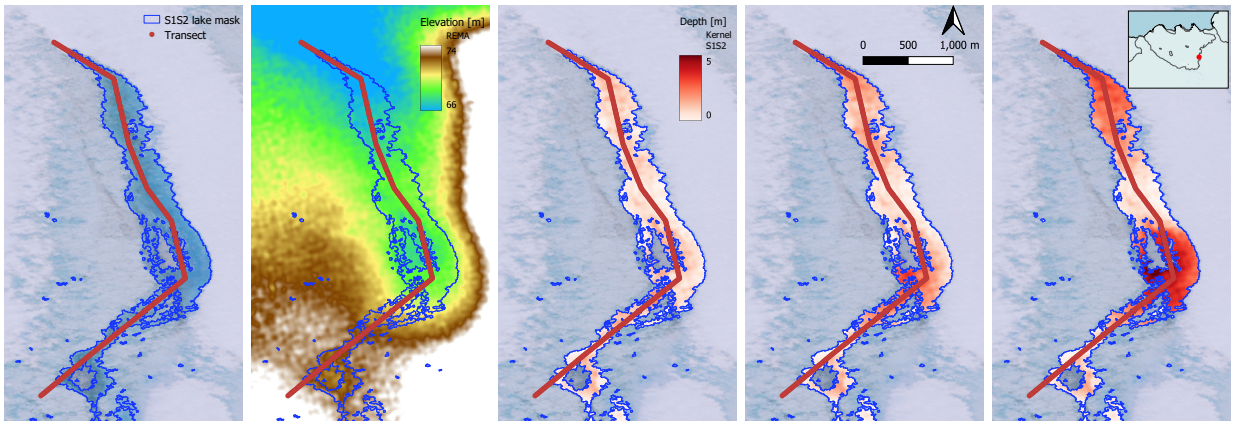

(a) (b) (c) (d) (e)

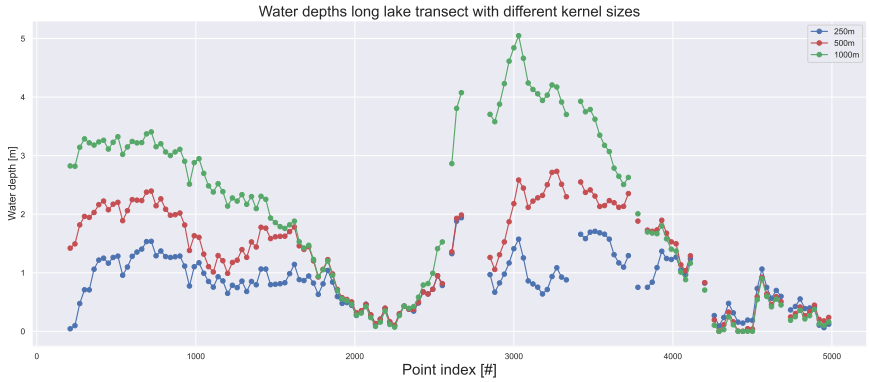

(f)

Figure 5.2.31: Sentinel-2 image, acquired on 17 December 2016 above Nivlisen, in true color (a), elevation according to REMA (b), the depths accoring kernel size 250 (c), 500 (d) and 1000m (e), results of the transect from southwest to northeast (f).

The largest lake on FeB 2019 is considerably less deep than the lakes shown earlier (figure 5.2.32). In this particular case, the cross-section runs from southwest to northeast. The 250 and 500-meter kernels show natural transitions. However, the 500 meter has great depths around edges in the northeast. The same holds for the 1000m in that area, but it the depths are even greater and the great depths around the edges are the case in the southwest and the middle.

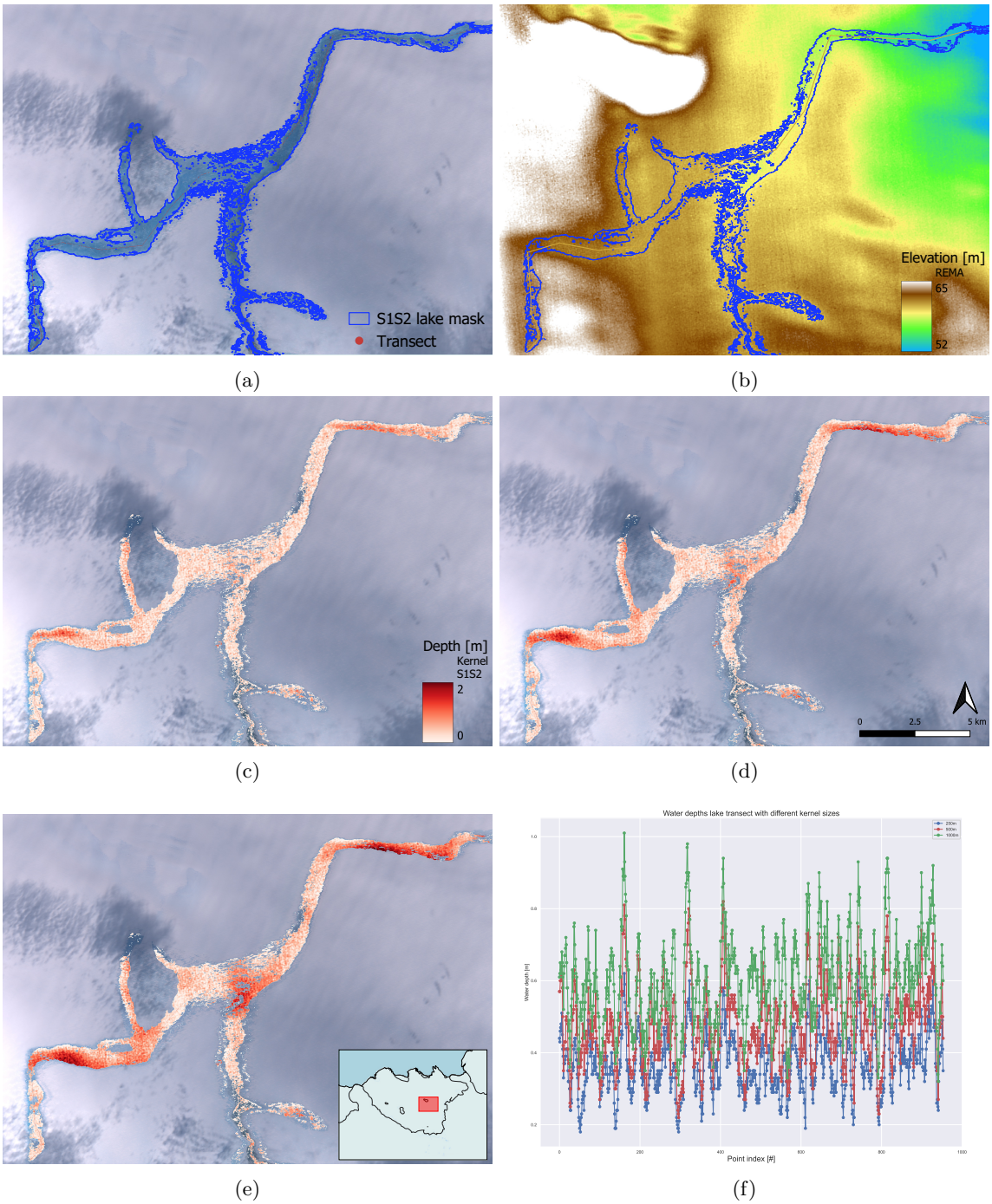

(a) (b) (c) (d) (e) (f)

Figure 5.2.32: Sentinel-2 image, acquired on 20 February 2019 above Nivlisen, in true color (a), elevation according to REMA (b), the depths accoring kernel size 250 (c), 500 (d) and 1000m (e), results of the transect from southwest to northeast (f).

5.2.2 Kernel and Reflectance methods

To analyse the depths, the means of the three methods were calculated. Next, all pixels of the geotiffs from the satellite methods were examined and a boxplot was made. Since the reflectance method was not able to calculate the depths of lakes larger than 1054 pixels, the calculations in 70m scale were also taken into account. Furthermore, some examples of depth calculations were visualised and explained with true color

representation and elevation.

When regarding the calculated means, an obvious observation is the overestimation of the RACMO method. Mean depths larger than 20 meters are not reasonable. Figure 5.2.34 shows the boxplots of the biweekly depths of the reflectance method 10 meters scale, kernel method size 250 meters, and reflectance method 70 meters scale, there are two things that immediately stand out. First, it is noticeable that the resulted depths based on the three different calculations are within the same magnitude range. There are however some outliers in all three cases. Secondly, scale 70 has greater depths than scale 10. On JanB2017 and JanA2018, the reflectance clearly has higher depths than the kernel. At these times there is relatively more water (figure 5.1.25), e.q. , and thus presence of large lakes, which are only visible with scale 70. A part of the large lake is shown in figure 5.2.33. Here it is clearly visible that the reflectance method overestimates the depth compared to the kernel method. When regarding the REMA, the depths of the kernel method seem on the small side. The reflectance method overestimates on e.q. JanB 2017 and JanA 2018, due to the presence of lakes larger than 1054 pixels. Those lakes influence the depths, as there are many pixels. In addition, this overestimation will affect the final volumes. Furthermore, it can be observed that the edges of the lakes based on the reflectance method with scale 70m look unnatural. By this is meant that the transition from inside the lake to the outer pixel is sharp caused by the coarser resolution.

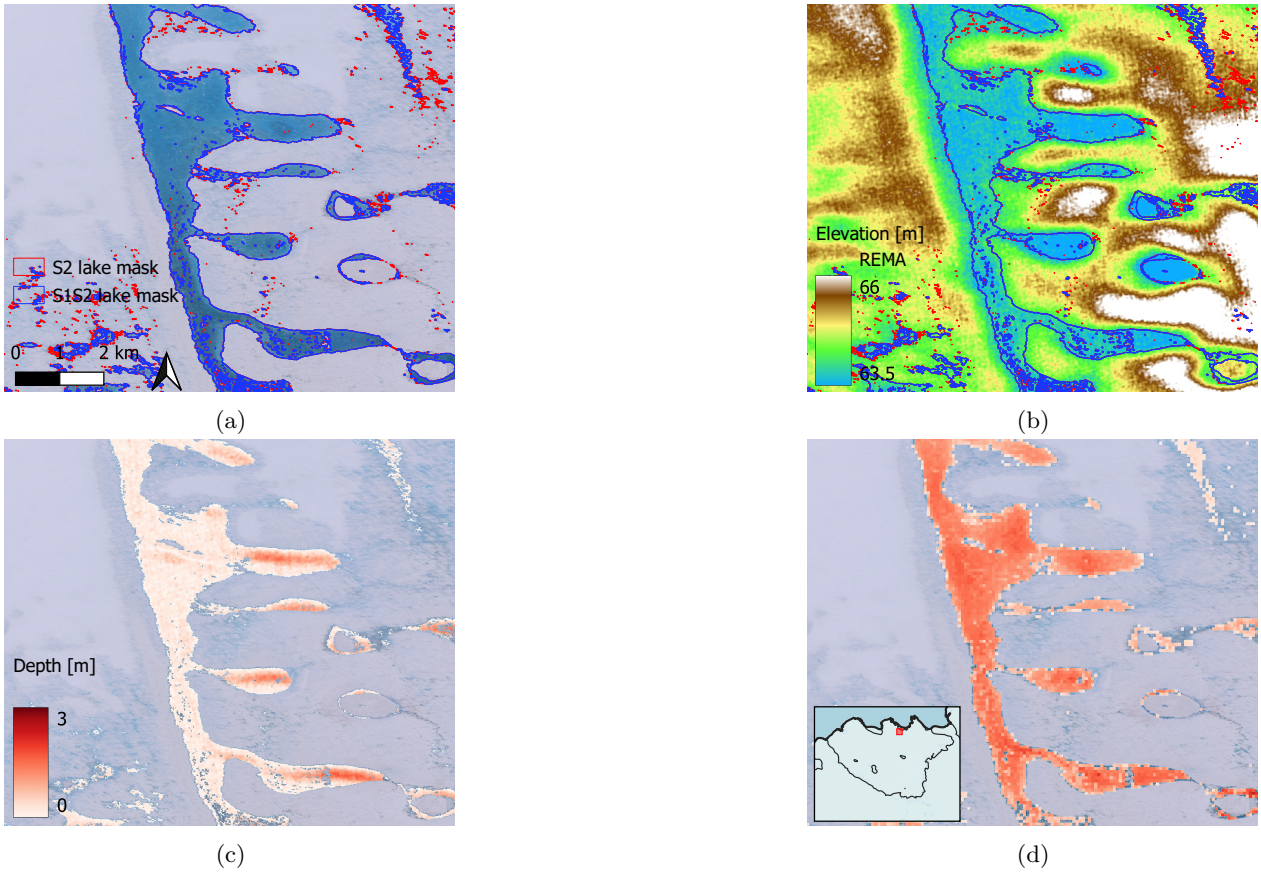

(a) (b) (c) (d)

Figure 5.2.33: Sentinel-2 image, acquired on 12 January 2018 above Nivlisen, in true color (a), elevation according to REMA (b) and depth using kernel method (c) and reflectance method with scale 70m (d) using S2 lake mask.

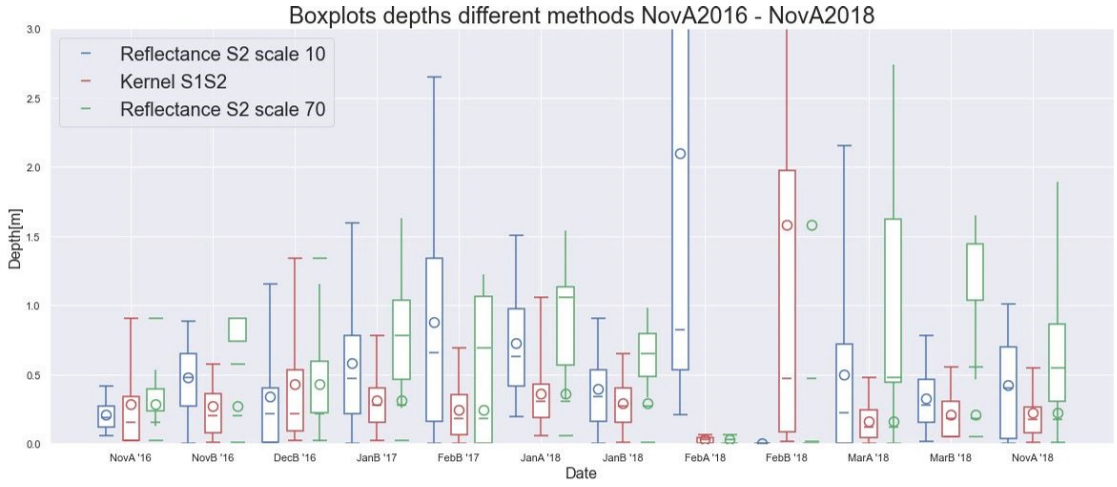

(a)

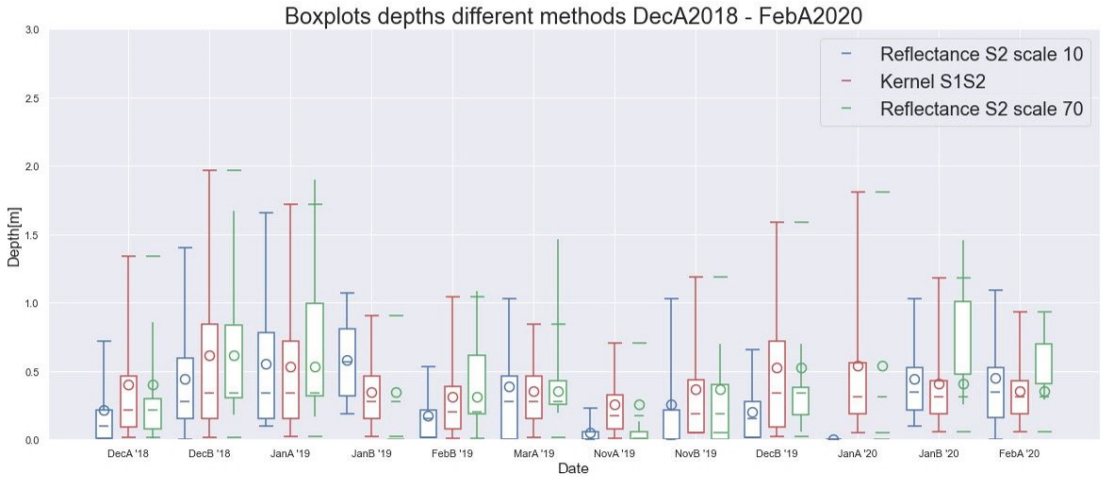

(b)

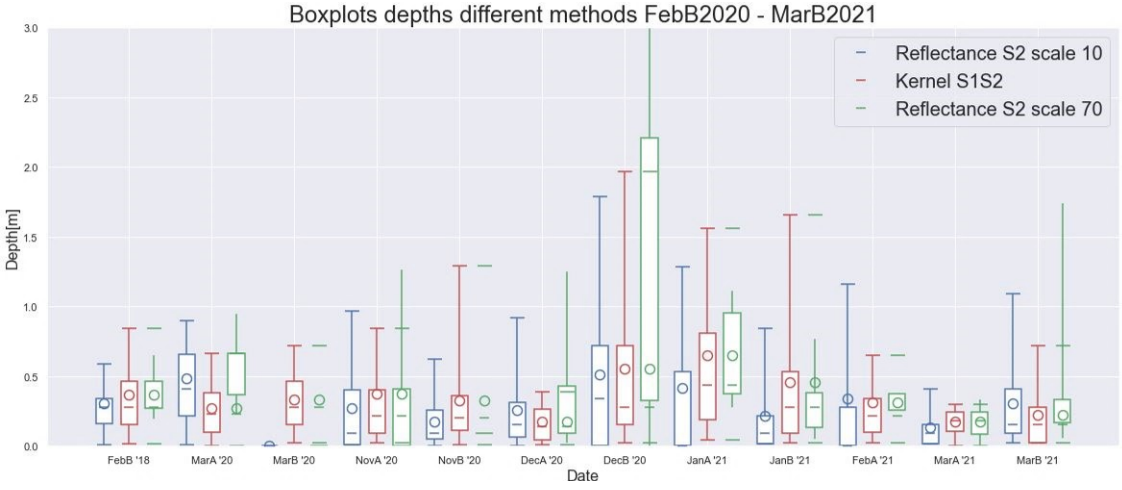

(c)

Figure 5.2.34: The boxplots of the depths according to the reflectance with S2 lake mask scale of 10m (a), kernel method with S1S2 lake mask (b) and reflectance with S2 lake mask scale of 70m (c)

Figure 5.2.35 displays the depths where the kernel is actually overestimating. The connected lakes are located between a steep slope and the kernel method is sensitive to hard elevation changes. It can be assumed that water will accumulate at the location with the lowest elevation, this is not entirely the case. Therefore, the DEM is not completely right corrected in some places, especially in the north-west, which increases the overestimation. The pond in the center east of the image is estimated deeper by the kernel method. However, the lake seems natural since it agrees with the REMA and the middle of the lake is the maximum depth and towards the edges almost to zero. Again, there are probably ice lids in most of the cavities in the circles, the REMA indicates lower or similar elevations in those places than in the places where there is water. ice lids

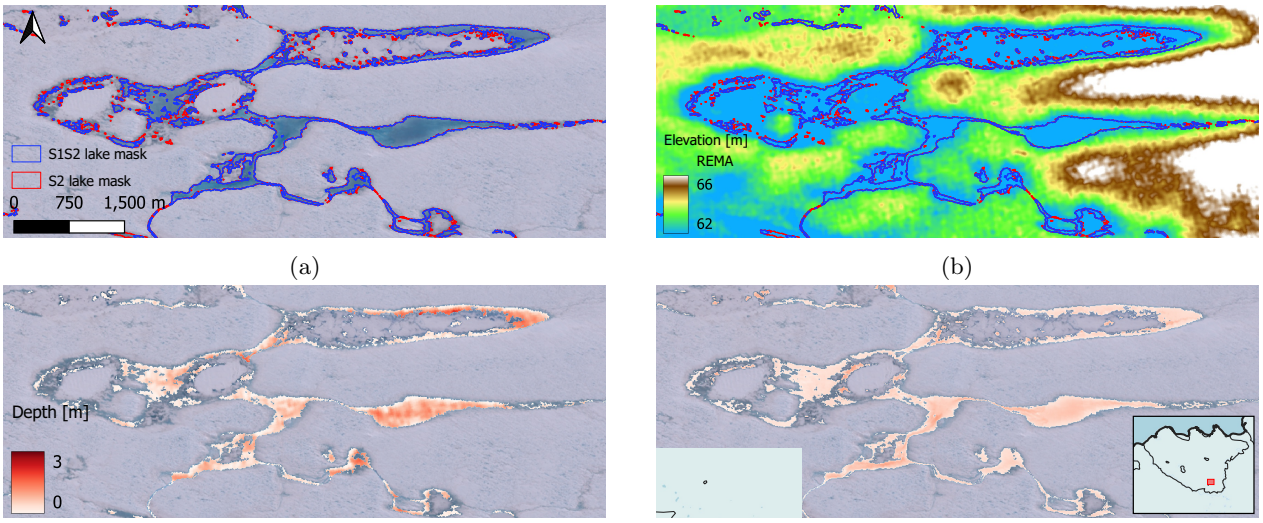

(a) (b)

(c) (d)

Figure 5.2.35: Sentinel-2 image, acquired on 26 January 2017 above Nivlisen, in true color (a), elevation according to REMA (b) and depth using kernel method (c) and reflectance method with scale 10m (d) using S2 lake mask.

5.3 Volume calculation

The purpose of this research was to develop a method to determine melt water as best as possible, therefore, volumes were calculated for the different methods. The overview of this for the five consecutive seasons is given in figure 5.3.36. From the figure, it can be observed that the pattern is comparable to that of the water extents (figure 5.1.25). However, it shows that the volumes resulting from the kernel method are greater than the ones calculated by the reflectance method. As was already shown in section 5.2, the depths calculated by use of the kernel method are smaller, which causes the same effect when determining the volumes. In addition, it shows that the RACMO data follows a similar pattern. At peak times during the melt season (DecB, JanA, JanB), the determined volume of water is significantly larger. The data from 2021 onwards are not included and so the melt water from that year is 0.

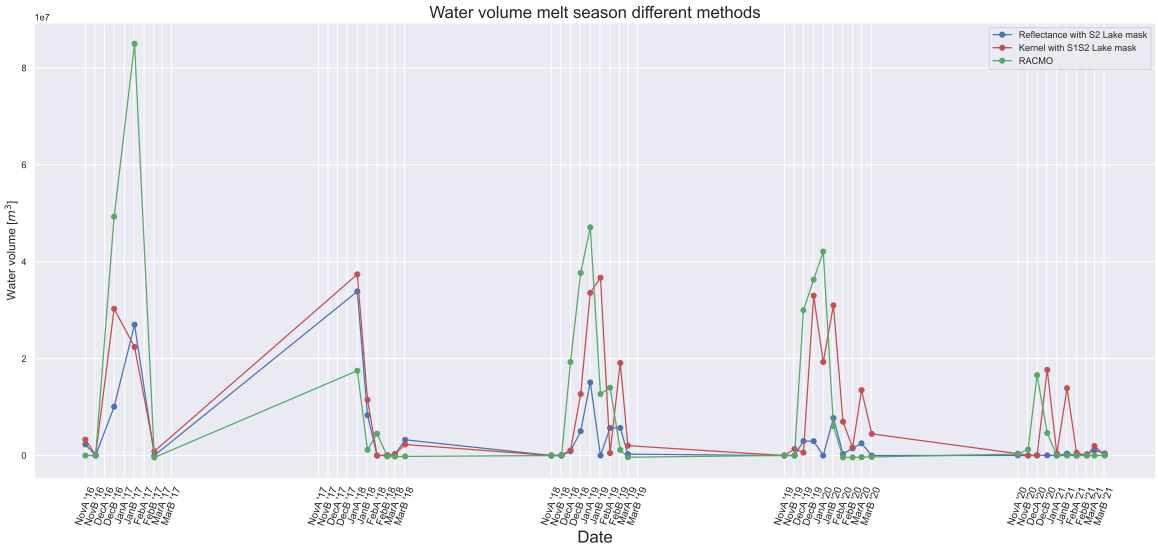

Figure 5.3.36: Volume melt water according to the three methods from 2016-2021

5.3.1 Comparison to Dell et al. (2020) and Van der Zalm (20)

In 2020, supraglacial lakes were also studied using RACMO and satellite data and these results are compared to those of this study. Dell et al. (2020) and Van der Zalm (2020) determined the area, average depths, and volumes during the 2016-2017 melt season. In addition to Sentinel-2, Landsat 7 was also used, providing more measurements.

In terms of surface area, the S1S2 lake mask comes close to that of Dell (2020). Compared to Van der Zalm (2020), both masks have 20 to 40 percent less extent. The average depths were a bit more difficult to determine, due to working with two scales for the reflectance method, however they overestimate considerably compared to Dell and a bit less compared to Van der Zalm. The depths of Dell (2020) and kernel method are close and follow the same pattern. The same can be said about the volumes and the surface: Kernel comparable to Dell (2020) and to Van der Zalm in December, but a substantial underestimate in January; Reflactance an underestimate relative to both methods in December and close to Dell (2020) in December. In contrast, the RACMO data has a higher volume, about the same as Van der Zalm (2020) in December and even around 25 percent higher in January.

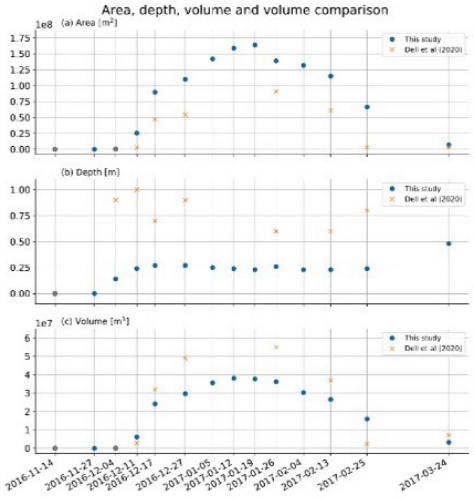

Figure 5.3.37: Area (a), depth (b) and volume (c) comparison of Van der Zalm (2020) indicated as this study and Dell et al. (2020)

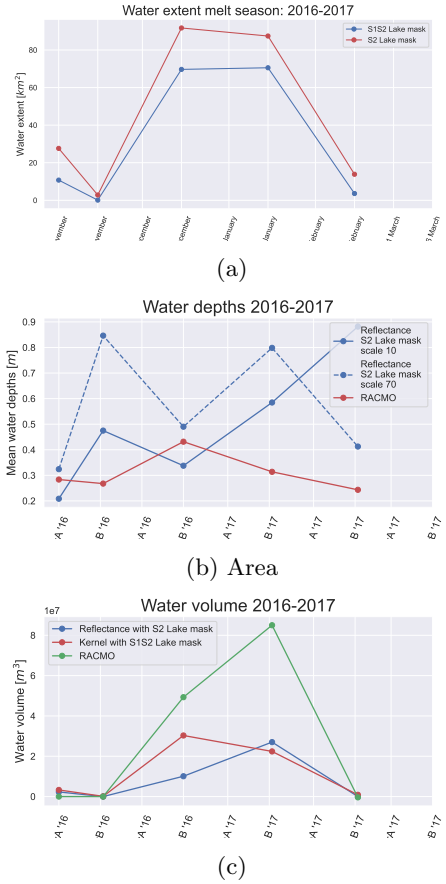

Figure 5.3.38: Area (a), depth (b) and volume (c) comparison of the three different methods in this study

6 Discussion

The discussion consists of two parts. Section 6.1 discusses this study in a wider context, in which the added value of the newly introduced methods and insights of existing techniques is discussed. Section 6.2 examines some of the decisions and assumptions that were made during this research.

6.1 Estimating meltwater volumes

The goal of this research was to be able to determine the volume of meltwater of supraglacial lakes in the most accurate way possible. The means was to expose and improve the limitations of satellite and climate model methods.

The method based on reflectance with S2 lake mask (method 1) produces realistic depths, less than 6 meters, and based on visual inspection of the true color composits the lakes mask classify accurately. This method was already existing and therefore it was useful to compare it to another method. However, examination of the influence of clouds on the scenes resulted in the fact that no filter could be used to increase the number of scenes and create a better estimation in water volumes. Visual inspection of the lake masks, elevation and true color images of the supraglacial lakes highlighted that ice lids are not classified as water, which resulted in an underestimation of water volume. Radar data is able to penetrate through the first layer of ice, however the Sentinel-1 part of the S1S2 lake mask is not equipped adequately enough to do so [Trusel et al., 2011].

A new method that was developed in this research is the kernel method. The method calculates depth by means of a lake mask and the elevation. The resulting magnitude of water depths are in the same range as the results from the reflectance method. However, there is still room for improvement in terms of the size of the kernel. In addition, the REMA will be more accurate if the exact date of the recording is known, which will also favor the results of the kernel method. The ability of the kernel method to determine the depth of the ice shelves by lake masking RADAR images offers great potential for better monitoring of the ice shelves. However, the kernel method will have to be tested on other ice shelves as well, before it can be used as an accurate method.

This study calculated the the depth, area and volume of supraglacial lakes with the aid of RACMO data. Determining the depths per pixel and water extent for the RACMO data was not successful. This would have had added value, because then it would be possible to compare these per pixel with the satellite methods. This would make it possible to better understand what possibly fails with the RACMO and the satellite methods. The climate model-based method of calculating the volume is similar to Van der Zalm (2020) based on catchment and therefore does not provide new insights.

6.2 Revision of results

This research shows three methods that result in a volume estimation of supraglacial lakes. However, the used different techniques are based on several assumptions that influence the accuracy of the outcomes. In this section, critical assumptions and other factors that constrain direct applicability of the results are discussed and comparisons are made with previous findings in literature. Firstly, the use of the water classification methods are discussed and compared in section 6.2.1. Secondly, the area and depth supraglacial lake derived based on RACMO is discussed in 6.2.2. Thirdly, the depth retrieval according to the satellite based methods are examined in section 6.2.3. Lastly, the total water volumes of the lakes were compared to one antoher and the differences are highlighted in section 6.2.4.

6.2.1 Comparing machine learning classifiers

Recent studies use supervised classification methods to locate the presence of supraglacial lakes. Most of these studies use threshold-based methods, for example Moussavi et al. (2020) and Halberstadt et al. (2016), who both studied supraglacial lakes using multispectral satellite products and Dirscherl et al. (2020), who mapped the melting ponds with multispectral satellite and SAR data. Fixed thresholds are used to distinguish ice, snow, rocks and water. In the case of multispectral satellite data, NDSI, NDWI, and spectral bands values

are used and in the case of SAR data in backscatter values are used. In this study both methods are executed on the Nivlisen Ice Shelf and compared to true color representations. The influence on the classification due to cloud cover using on the method of Moussavi et al. (2020) is examined.

Both threshold-based and machine learning classifiers have their advantages and disadvantages. The results of the classification maps look very similar based on visual inspection and agreement in pixels as described in section 5.1.2. According to Moussavi et al. (2020) the average accuracy is approximately 97.5%. Both lake masks seem to detect what appear to be ice lids, as non-water. In terms of of classification this is correct, since the surface is frozen. However, when the focus is on determining the water volume of supraglacial lakes, thes ice lids are desired to be classified as water, as there is water present underneath the ice surface.

The S2 lake mask is less strict than the S2 part of the S1S2 lake mask, which can be seen in figure 5.1.26. For JanB 2017 and JanA 2018 the S2 lake mask detects more water, while both methods use the same Sentinel-2 scene based on equal cloud cover filtering. Hence, it can be said that the S2 part of the S1S2 lake mask is more strict. Based on visual inspection it was observed that the overestimation was correctly classified.

Studying the classification maps in combination with the true color representations of the S2 scenes and the total water extent time series (figure 5.1.25), it was observed that the S1 part of the S1S2 lake mask does not provide more information in comparison to the S2 part. This can for example be observerd when comparing JanB '17 and JanA '18: here, the S2 lake mask detects more thbe seen that in e.g. JanB 2017 and JanA 2018 S2 lake mask detects more water than the S1S2 lake mask. The S1S2 lake mask make use of direct backscatter thresholds. There is not much difference in backscatter between aswell slush and water aswell frozen ice lid and water in terms of backscatter. However, melt can be detected more accurately when using indirect radar images. This method is also able to detect whether there is an ice lid [Trusel et al., 2011].

The classification methods use biweekly extents. The S2 lake mask often uses only one scene, simply because only one is available every two weeks. In contrast, this is not the case for the S1S2 lake mask, which makes comparison based on S2 images difficult. The S1 image was processed at a different time than the S2 image. In addition, it is not clear which pixel is classified as water based on the S1 or the S2 scenes. Hence, if a pixel is classified as water according to the lake mask, but is not visible on the S2 image, one cannot determine if that classification is wrong or right.

The degree to which cloud cover affects the optical data can be divided into two ways. First, due to the fact that the presence of the cloud pixels underneath are not visible and so cannot be detected as water. Second, the possibility of misclassification increases due to the of shadow clouds. It would be recommended to not use a cloud filter. JanB19's moment indicates that there can be considerable underestimation by filtering a scene out, even when there are no clouds present above the supraglacial lakes. In addition, the wrongly classified shadow of the clouds does not have that much influence [Moussavi et al., 2020]. It is better to risk slight overestimation than to cause sever underestimation. Especially when regarding vulnerability of the ice shelf due to hydrofracturing, the worst case scenerio is leading.

The problem with this comparison, however, is that there is no "ground truth". Based on visual inspection, it is possible to judge whether something is probably true or not. There is more probability if the two classifications coincide, but there is no absolute truth. The best option would be to validate the methods with in-situ data from the AWS. Another option is to compare the methods with a method that is fundamentally different, which will provide more insights.

6.2.2 Locating and estimating depth supraglacial lake with a regional climate model

Several studies use regional climate models to estimate meltwater volumes. eerdere studies hebben hoeveelheid smeltwater bepaald. deze studie: waterlichamen the mappen en in te schatten. The Modele Atmospherique Regional (MAR) [Arenson and Colgan, 2015] and the regional climate model (RACMO) [van Wessem et al., 2018] calculate several parameters per location from which the total runoff over a region of interest is estimated. In this study the flow of meltwater and the location of accumulation was calculated

using python module *pysheds*.

The RFSM function in pysheds calculates where the amount of runoff accumulates. According to the results of the area and the mean depth calculations, it can be stated that the method is not working as expected. The depths are tens of meters and the water extent is 10 times larger than depths according to satellite-based techniques. A possible cause is the spatial resolution of the DEM (500m) and RACMO (27km). The RFSM method was not capable of running the region of interest on a higher resolution due to computational costs. The coarse DEM resolution possible results in wrong mapping of the depression locations where the water accumulates, since supraglacial lakes are often smaller than 500 m in width, length or even both. A better resolution of RACMO data of this version needs to be validated and therefore is not taken into account in this study. The resolution averages the same runoff values over an area of 27 by 27 kilometers, it can be the case that the processes change locally.

RACMO does not take draining of meltwater into account in the calculation of meltwater. The problem is that meltwater that arises possibly immediately drains away and then the next day water may arise in that spot again which again drains away and so on. It is possible, for example, that water will drain towards a much lower location with a lower temperature, where it would not refreeze and thus would influence the amount of meltwater. In this case, it is bucket that is filled for a period of weeks or months and pore over it on a given day. In the real world the water drains away during the time in between the release and the build up moment. So for the future try in RACMO or a good way of doing the hydrological model. It is recommended to calculate the drain inside the RACMO model or a method to couple the draining mechanims with the outcome of RACMO.

There is a great advantage in allocating the supraglacial lakes and estimating the depth of the supraglacial lakes due to the possibility to predict vulnerabilities of ice shelves. Knowing the mass of the lakes will aid to understand the forces that are present on the ice shelf. The temporal resolution is daily and it can estimate in the future, which helps to understand the possible problems due to hydrofracturing on ice shelves. Therefore, detecting and magnifying supraglacial lakes with regional climate model is promising.

6.2.3 Satellite-based depth retrieval

State of the art methods use satellite data to retrieve the depth of supraglacial lakes. [Moussavi et al., 2020] uses the principle that light passing through water is scattered or absorbed and calculates the depth via an equation from [Philpot, 1989]. These methods are based on optical satellite data. The method using the equation of [Philpot, 1989], the reflectance method, is used and evaluated in this research. A new method was developed in this study, the kernel method, which is not dependent on satellite data. It instead uses a lake mask and the DEM. In order to gain more insights in this method, a sensitivity analysis was executed containing different sizes of the kernel.

Both methods have different advantages and disadvantages, but, according to the data, the values of both methods are in the same ball park.. The reflectance method is already validated and verified in earlier studies on different ice shelves on the AIS. A disadvantage of this method is that it is dependent on optical data. The temporal resolution is 12 days and the presence of clouds could lower the resolution. An advantage of the kernel method is that it could be applied to every lake mask, e.q. optical and radar satellite data. Therefore, the amount of usable data is greater than that of the reflectance method.

The reflectance method is influenced by atmospheric conditions. For example, if it is foggy, a different depth is estimated than if it is not foggy. The different depths causing an increase in uncertainty and one have to consult the true color representation to check the presence of fog. Furthermore, it is not possible to look under ice lids and clouds, since it cannot penetrate through. By use of interpolation the depth could be estimated, however, that also brings uncertainties depending on the interpolation technique.

The kernel method has the disadvantage that it is dependent on the DEM and the DEM is constantly changing due to ice flow. In this case, the exact date is not available each time, because the S1S2 lake mask

calculated a biweekly extent. In addition, the S1 and S2 images are at different times. The DEM is therefore not corrected for the same date as the acquisitions, this increases the uncertainty in determining the precise DEM and so the depth. Also, the velocity model is a coarser resolution, 120m, which has negatively influences the correctness of the DEM.

Kernel sizes have considerable influence. The larger the window the greater the likelihood of great depth. Ideally it changes of size per lake. Preferably over the width of the lake or to centerline. The edges of the supraglacial lakes will become approximately 0. SHORT: kernel improvement and testing with validation data and checking that, has more future than reflectance method.

Again there is no ground truth present which impedes the validation and verification of both methods. The methods can be tested on greater scale on other ice shelves to gain more insight, since other ice shelves bring other circumstances. Possibly using AWS or field measurements to compare in-situ measurements with the depth retrieval methods.

6.2.4 Total volume of supraglacial lakes

The total supraglacial lake volumes according to the different methods are within in the same range. The overestimation by RACMO is possibly causded since it uses the maximum amount of runoff in two weeks. The satellite data takes the maximum extent over two to five scenes, while RACMO is able to calculate the runoff of every day. The catchments are also causing uncertainty, based on Geerten et al. (2020) to catchements. The coarse resolution of RACMO, 27km, has influence on the certainty. It is plausible that the catchment cuts through a pixel. Then the value is assigned for the entire tile. The runoff in the area that falls inside the catchment may have a very different runoff than the area that falls outside it, yet it will have the same value. On the other hand, the uncertainties for determining volumes using satellite methods are mainly caused by the depth and area determinations. These complications have already been discussed in the sections above.

7 Conclusion

This study assessed the volume estimation of supraglacial lakes on the AIS potentials and limitations of satellite-based and regional climate-based models. The key findings obtained during this study are presented in Section 7.1. First, the sub-questions are discussed, followed by the main research question. During this thesis research, hypotheses were developed for the determining the area, depth and volumes. Not all of these hypotheses could be accepted. However, there are also some proposed improvements, see Section 6.2. Finally, three recommendations for future research are listed in Section 8.

7.1 Key findings

What are the spatiotemperal patterns in detecting lake presence between the different satellite methods
A threshold-based machine learning approach for supraglacial lakes that is completely correct is not feasible, yet it must be pursued. In this research two methods are used, S2 lake mask (method 1) and S1S2 lake mask (method 2). The two masks are not very different, apart from the shadows, which can be partially solved by a others NDWI value. It seems that the S2 part of the S1S2 lake mask underestimates due to the fact that it is to strict and the S2 lake mask operates better in that way. However, the masks have the same problems with respect to refrozen parts of the lakes. Better use of S1, measuring the backscatter indirectly, should make this possible [Trusel et al., 2011].

The ponds detection is affected by clouds in two ways. On the one hand, the recording can be declared unusable because a threshold for cloud coverage may have been set. In addition, the water that is underlying cannot be detected, since the light cannot penetrate trough the cloud. On the other hand, the presence of clouds causes shadowing and which in turn increases the probability of missclasification. Based on visual inspection in this research the missclassification do not happen that much and according to Moussavi et al. (2020) the NDWI threshold set on 0.3 solves this problem.

How can meltwater volumes be derived using non-optical satellite data?
A depth retrieval algorithm that is used for all types satellite data is not been developed. Optical solutions have problems due to clouds and ice lids. In this thesis, a new method is developed, which is able to determine lake depths of non-optical satellite data, and studied.

Using the kernel method it is possible to determine lakes with only a lake mask and a DEM. The highest elevated pixel of the lake within the kernel is equal to the water table. Then the depth is calculated by subtracting the elevation from the top of the water table. Therefore this method is able to be used on any data that can produce or is a lake mask, so non-optical satellite data as well. An advantage of using SAR data is that the determination can be done independent of clouds. In addition, it is possible to determine the depth under the ice lids, due to the fact that SAR can detect underneath the frozen surface [Trusel et al., 2011].

The size of the kernel has influence on the maginitudes of the depths. Based on the senstivity analysis in section Sensitivity Analysis: kernel sizes, it can be concluded that the larger the kernelsize the greater depth. The chance that a higher elevated pixel is in the kernel increases with size and so the possibility of greater depths. However, there is still room for improvement in terms of kernel sizes.

The kernel method shows great potential in order to determine the depths of supraglacial lakes. *What are the possibilities of determining the volume of individual water bodies using a Regional climate Model*
Untill this research solely the total volume meltwater over a region of interest was calculated. In this study the depth, area and volume per pond were calculated. The results of the climated-based method (method 3) were compared with two satellite-based methods (methods 1 and 2).

The total amount of meltwater is calculated with the parameters snowmelt, refreezing, precipitation and snowfall derived from RACMO. The catchment of the supraglacial lakes is then determined with the aid of the DEM and the module *Pysheds*. The total volume of meltwater is calculated by taking the sum of the runoff within that catchment and compared to the volumes calculated by the other methods. It seems that

the volume is overestimated in comparisson to the satellite-based methods, getal, this is possibly due to the fact that the RACMO calculates the maximum over all the days of the twee weeks and a part flows towards non-supraglacial lakes near the grounding line. Nevertheless, the outcomes of the three methods by means of total volume supraglacials are in the same order of magnitude.

However, the calculated depths and areas of the supraglacial lakes according to method 3 are not in the same range in comparison to the satellite-based methods. The depths (+ 30m on average) and the areas (10 times more than the satellite-methods) are unrealistic and therefore this method is not considered successful. Potential causes for these numbers are the coarse resolution of the corrected DEM (500m) and the RACMO data (27km). Calculating the depth and location of melting ponds with a regional climate model, seems to be promessing due to the fact that the temporal resolution is high (daily) and its possibility to predict the lakes in the future, which gain certainty in the vulnerability of ice shelves in the coming decades.

References

[Lai, 2020] (2020). Vulnerability of antarctica's ice shelves to meltwater-driven fracture. *Nature*, 584(7822):574–578.

[Arenson and Colgan, 2015] Arenson, L. and Colgan, W. (2015). Water management challenges associated with mining projects in greenland.

[Arthur et al., 2020] Arthur, J. F., Stokes, C., Jamieson, S. S., Carr, J. R., and Leeson, A. A. (2020). Recent understanding of antarctic supraglacial lakes using satellite remote sensing. *Progress in Physical Geography: Earth and Environment*, 44(6):837–869.

[Banwell et al., 2013] Banwell, A. F., MacAyeal, D. R., and Sergienko, O. V. (2013). Breakup of the larsen b ice shelf triggered by chain reaction drainage of supraglacial lakes. *Geophysical Research Letters*, 40:5872–5876. Interessante hypothese over hoe een hydrofracturing event voor ¡br/¿weer nieuwe hydrofracturing events kan zorgen (chain reaction).

[Bell, 2018] Bell, R., B. A. T. L. . K. J. (2018). Antarctic surface hydrology and impacts on ice-sheet mass balance. *Nature Climate Change*, 8(21):1044–1052.

[Buzzard et al., 2018] Buzzard, S., Feltham, D., and Flocco, D. (2018). A mathematical model of melt lake development on an ice shelf. *Journal of Advances in Modeling Earth Systems*, 10.

[Buzzard and Robel, 2020] Buzzard, S. and Robel, A. (2020). A 3-D Model of Antarctic Ice Shelf Surface Hydrology. In *EGU General Assembly Conference Abstracts*, EGU General Assembly Conference Abstracts, page 278.

[Church et al., 2013] Church, J., Clark, P., Cazenave, A., Gregory, J., Jevrejeva, S., Levermann, A., Merrifield, M., Milne, G., Nerem, R., Nunn, P., Payne, A., Pfeffer, W., Stammer, D., and Unnikrishnan, A. (2013). *Sea Level Change*, book section 13, page 1137–1216. Cambridge University Press, Cambridge, United Kingdom and New York, NY, USA.

[Cook and Vaughan, 2010] Cook, A. J. and Vaughan, D. G. (2010). Overview of areal changes of the ice shelves on the antarctic peninsula over the past 50 years. *The Cryosphere*, 4(1):77–98.

[Dell et al., 2020] Dell, R., Arnold, N., Willis, I., Banwell, A., Williamson, A., Pritchard, H., and Orr, A. (2020). Lateral meltwater transfer across an antarctic ice shelf. *The Cryosphere*, 14:2313–2330.

[Dirscherl et al., 2020] Dirscherl, M., Dietz, A. J., Kneisel, C., and Kuenzer, C. (2020). Automated mapping of antarctic supraglacial lakes using a machine learning approach. *Remote Sensing*, 12(7).

[Dirscherl et al., 2021a] Dirscherl, M., Dietz, A. J., Kneisel, C., and Kuenzer, C. (2021a). A novel method for automated supraglacial lake mapping in antarctica using sentinel-1 sar imagery and deep learning. *Remote Sensing*, 13(2).

[Dirscherl et al., 2021b] Dirscherl, M. C., Dietz, A. J., and Kuenzer, C. (2021b). Seasonal evolution of antarctic supraglacial lakes in 2015–2021 and links to environmental controls. *The Cryosphere*, 15(11):5205–5226.

[Fair et al., 2020] Fair, Z., Flanner, M., Brunt, K. M., Fricker, H. A., and Gardner, A. (2020). Using icesat-2 and operation icebridge altimetry for supraglacial lake depth retrievals. *The Cryosphere*, 14(11):4253–4263.

[Fretwell et al., 2013] Fretwell, P., Pritchard, H. D., Vaughan, D. G., Bamber, J. L., Barrand, N. E., Bell, R., Bianchi, C., Bingham, R. G., Blankenship, D. D., Casassa, G., Catania, G., Callens, D., Conway, H., Cook, A. J., Corr, H. F. J., Damaske, D., Damm, V., Ferraccioli, F., Forsberg, R., Fujita, S., Gim, Y., Gogineni, P., Griggs, J. A., Hindmarsh, R. C. A., Holmlund, P., Holt, J. W., Jacobel, R. W., Jenkins, A., Jokat, W., Jordan, T., King, E. C., Kohler, J., Krabill, W., Riger-Kusk, M., Langley, K. A., Leitchenkov, G., Leuschen, C., Luyendyk, B. P., Matsuoka, K., Mouginot, J., Nitsche, F. O., Nogi, Y., Nost, O. A., Popov, S. V., Rignot, E., Rippin, D. M., Rivera, A., Roberts, J., Ross, N., Siegert, M. J., Smith, A. M.,

Steinhage, D., Studinger, M., Sun, B., Tinto, B. K., Welch, B. C., Wilson, D., Young, D. A., Xiangbin, C., and Zirizzotti, A. (2013). Bedmap2: improved ice bed, surface and thickness datasets for antarctica. *The Cryosphere*, 7:375–393.

[Fricker et al., 2021] Fricker, H. A., Arndt, P., Brunt, K. M., Datta, R. T., Fair, Z., Jasinski, M. F., Kingslake, J., Magruder, L. A., Moussavi, M., Pope, A., Spergel, J. J., Stoll, J. D., and Wouters, B. (2021). Icesat-2 meltwater depth estimates: Application to surface melt on amery ice shelf, east antarctica. *Geophysical Research Letters*, 48(8):e2020GL090550. e2020GL090550 2020GL090550.

[Fürst et al., 2016] Fürst, J. J., Durand, G., Gillet-Chaulet, F., Tavard, L., Rankl, M., Braun, M., and Gagliardini, O. (2016). The safety band of antarctic ice shelves. *Nature Climate Change*, 6:479–482.

[Gascon et al., 2014] Gascon, F., Cadau, E., Colin, O., Hoersch, B., Isola, C., Fernández, B., and Martimort, P. (2014). Copernicus sentinel-2 mission: Products, algorithms and cal/val. volume 9218.

[Horwath et al., 2006] Horwath, M., Dietrich, R., Baessler, M., Nixdorf, U., Steinhage, D., Fritzsche, D., Damm, V., and Reitmayr, G. (2006). Nivlisen, an antarctic ice shelf in dronning maud land: geodetic–glaciological results from a combined analysis of ice thickness, ice surface height and ice-flow observations. *Journal of Glaciology*, 52(176):17–30.

[Howat et al., 2019] Howat, I. M., Porter, C., Smith, B. E., Noh, M.-J., and Morin, P. (2019). The reference elevation model of antarctica. *The Cryosphere*, 13(2):665–674.

[Hu et al., 2021] Hu, Z., Kuipers Munneke, P., Lhermitte, S., Izeboud, M., and van den Broeke, M. (2021). Improving surface melt estimation over the antarctic ice sheet using deep learning: a proof of concept over the larsen ice shelf. *The Cryosphere*, 15(12):5639–5658.

[Jonsell et al., 2011] Jonsell, U., Navarro, F., Bañon, M., Lapazaran, J., and Otero, J. (2011). Sensitivity of a distributed temperature-radiation index melt model based on a four melt season aws record from hurd peninsula glaciers, livingston island, antarctica. *The Cryosphere Discussions*, 5:3221–3258.

[Kingslake et al., 2015] Kingslake, J., Ng, F., and Sole, A. (2015). Modelling channelized surface drainage of supraglacial lakes. *Journal of Glaciology*, 61(225):185–199.

[Kotawadekar, 2021] Kotawadekar, R. (2021). 9 - satellite data: big data extraction and analysis. In Binu, D. and Rajakumar, B., editors, *Artificial Intelligence in Data Mining*, pages 177–197. Academic Press.

[Lenaerts et al., 2017] Lenaerts, J., Lhermitte, S., Drews, R., Ligtenberg, S., Berger, S., Helm, V., Smeets, C., van den Broeke, M., van de Berg, W., van Meijgaard, E., Eijkelboom, M., Eisen, O., and Pattyn, F. (2017). Meltwater produced by wind–albedo interaction stored in an east antarctic ice shelf. *Nature Climate Change*, 7:58–62.

[Lenaerts et al., 2014] Lenaerts, J. T., Brown, J., Van Den Broeke, M. R., Matsuoka, K., Drews, R., Callens, D., Philippe, M., Gorodetskaya, I. V., Van Meijgaard, E., Reijmer, C. H., and et al. (2014). High variability of climate and surface mass balance induced by antarctic ice rises. *Journal of Glaciology*, 60(224):1101–1110.

[Lenaerts et al., 2018] Lenaerts, J. T. M., Ligtenberg, S. R. M., Medley, B., Van de Berg, W. J., Konrad, H., Nicolas, J. P., Van Wessem, J. M., Trusel, L. D., Mulvaney, R., Tuckwell, R. J., and et al. (2018). Climate and surface mass balance of coastal west antarctica resolved by regional climate modelling. *Annals of Glaciology*, 59(76pt1):29–41.

[Lhermitte et al., 2020] Lhermitte, S., Sun, S., Shuman, C., Wouters, B., Pattyn, F., Wuite, J., Berthier, E., and Nagler, T. (2020). Damage accelerates ice shelf instability and mass loss in amundsen sea embayment. *Proceedings of the National Academy of Sciences*, 117:24735–24741. Pine island glacer and the Thwaites Glacier are in the west of Antartica in below the peninsula.

[Lindbäck et al., 2019] Lindbäck, K., Moholdt, G., Nicholls, K. W., Hattermann, T., Pratap, B., Thamban, M., and Matsuoka, K. (2019). Spatial and temporal variations in basal melting at nivlisen ice shelf, east antarctica, derived from phase-sensitive radars. *The Cryosphere*, 13(10):2579–2595.

[Meredith and King, 2005] Meredith, M. and King, J. (2005). Rapid climate change in the ocean west of the antarctic peninsula during the second half of the 20th century. *Geophysical Research Letters - GEOPHYS RES LETT*, 32.

[Moussavi et al., 2020] Moussavi, M., Pope, A., Halberstadt, A. R. W., Trusel, L. D., Cioffi, L., and Abdalati, W. (2020). Antarctic supraglacial lake detection using landsat 8 and sentinel-2 imagery: Towards continental generation of lake volumes. *Remote Sensing*, 12(1).

[Munneke et al., 2014] Munneke, P. K., Ligtenberg, S. R., Broeke, M. R. V. D., and Vaughan, D. G. (2014). Firn air depletion as a precursor of antarctic ice-shelf collapse. *Journal of Glaciology*, 60:205–214. Duidelijke uitleg over de rol van de firn laag in ice shelf collapses.

[Philpot, 1989] Philpot, W. (1989). Bathymetric mapping with passive multispectral imagery. *Applied optics*, 28:1569–78.

[Pope et al., 2016] Pope, A., Scambos, T., Moussavi, M., Tedesco, M., Willis, M., Shean, D., and Grigsby, S. (2016). Estimating supraglacial lake depth in west greenland using landsat 8 and comparison with other multispectral methods. *The Cryosphere*, 10:15–27.

[Rignot et al., 2004] Rignot, E., Casassa, G., Gogineni, P., Krabill, W., Rivera, A., and Thomas, R. (2004). Accelerated ice discharge from the antarctic peninsula following the collapse of larsen b ice shelf. *Geophysical Research Letters*, 31(18).

[Rignot et al., 2011] Rignot, E., Mouginot, J., and Scheuchl, B. (2011). Ice flow of the antarctic ice sheet. *Science*, 333(6048):1427–1430.

[Rignot et al., 2019] Rignot, E., Mouginot, J., Scheuchl, B., van den Broeke, M., van Wessem, M. J., and Morlighem, M. (2019). Four decades of antarctic ice sheet mass balance from 1979–2017. *Proceedings of the National Academy of Sciences*, 116(4):1095–1103.

[Scambos et al., 2004] Scambos, T., Bohlander, J., Shuman, C., and Skvarca, P. (2004). Glacier acceleration and thinning after ice shelf collapse in the larsen b embayment, antarctica. *Geophysical Research Letters*, 31.

[Stokes et al., 2019] Stokes, C., Sanderson, J., Miles, B., Jamieson, S., and Leeson, A. (2019). Widespread distribution of supraglacial lakes around the margin of the east antarctic ice sheet. *Scientific Reports*, 9:1–14.

[Tapley et al., 2019] Tapley, B., Watkins, M., Flechtner, F., Reigber, C., Bettadpur, S., Rodell, M., Sasgen, I., Famiglietti, J., Landerer, F., Chambers, D., Reager, J., Gardner, A., Save, H., Ivins, E., Swenson, S., Boening, C., Dahle, C., Wiese, D., Dobslaw, H., and Velicogna, I. (2019). Contributions of grace to understanding climate change. *Nature Climate Change*, 5.

[the IMBIE team, 2018] the IMBIE team (2018). Analysis insight. *Nature*, 558:219–222.

[Torres et al., 2012] Torres, R., Snoeij, P., Davidson, M., Bibby, D., and Lokas, S. (2012). The sentinel-1 mission and its application capabilities. pages 1703–1706.

[Trusel et al., 2011] Trusel, L., Frey, K., and Das, S. (2011). Antarctic surface melting dynamics: Enhanced perspectives from radar scatterometer data. *AGU Fall Meeting Abstracts*, 117:0596–.

[Urruty et al., 2022] Urruty, B., Hill, E. A., Reese, R., Garbe, J., Gagliardini, O., Durand, G., Gillet-Chaulet, F., Gudmundsson, G. H., Winkelmann, R., Chekki, M., Chandler, D., and Langebroek, P. M. (2022). The stability of present-day antarctic grounding lines – part a: No indication of marine ice sheet instability in the current geometry. *The Cryosphere Discussions*, 2022:1–34.

[van Wessem et al., 2018] van Wessem, J. M., van de Berg, W. J., Noël, B. P. Y., van Meijgaard, E., Amory, C., Birnbaum, G., Jakobs, C. L., Krüger, K., Lenaerts, J. T. M., Lhermitte, S., Ligtenberg, S. R. M., Medley, B., Reijmer, C. H., van Tricht, K., Trusel, L. D., van Ulft, L. H., Wouters, B., Wuite, J., and van den Broeke, M. R. (2018). Modelling the climate and surface mass balance of polar ice sheets using racmo2 – part 2: Antarctica (1979–2016). *The Cryosphere*, 12(4):1479–1498.

[Williamson et al., 2018] Williamson, A., Banwell, A., Willis, I., and Arnold, N. (2018). Dual-satellite (sentinel-2 and landsat 8) remote sensing of supraglacial lakes in greenland. *The Cryosphere*, 12:3045–3065.